Molecular Therapy
Original Article

A Stem Cell-Based Screening Platform Identifies Compounds that Desensitize Motor Neurons to Endoplasmic Reticulum Stress

Sebastian Thams,[1,9] Emily Rhodes Lowry,[1,7] Marie-Hélène Larraufie,[2,7,10] Krista J. Spiller,[1,8] Hai Li,[1] Damian J. Williams,[3] Phuong Hoang,[1] Elise Jiang,[2] Luis A. Williams,[4] Jackson Sandoe,[4] Kevin Eggan,[4] Ivo Lieberam,[5] Kevin C. Kanning,[1] Brent R. Stockwell,[2] Christopher E. Henderson,[1,11] and Hynek Wichterle[1,6]

[1]Department of Pathology and Cell Biology, Center for Motor Neuron Biology and Disease, Columbia Stem Cell Initiative, Columbia University Irving Medical Center, 630 West 168th Street, New York, NY 10032, USA; [2]Department of Biological Sciences and Department of Chemistry, Columbia University, Northwest Corner Building, MC4846, 550 West 120th Street, New York, NY 10027, USA; [3]Department of Physiology and Cellular Biophysics, Columbia University Irving Medical Center, 650 West 168th Street, New York, NY, USA; [4]Department of Stem Cell and Regenerative Biology, Harvard University, MA 02138, USA; [5]Centre for Stem Cells and Regenerative Medicine and MRC Centre for Neurodevelopmental Disorders, King's College London, London SE1 9RT, UK; [6]Departments of Neuroscience, Rehabilitation and Regenerative Medicine, and Neurology, Columbia University Irving Medical Center, 630 West 168th Street, New York, NY 10032, USA

Amyotrophic lateral sclerosis (ALS) is a neurodegenerative disease selectively targeting motor neurons in the brain and spinal cord. The reasons for differential motor neuron susceptibility remain elusive. We developed a stem cell-based motor neuron assay to study cell-autonomous mechanisms causing motor neuron degeneration, with implications for ALS. A small-molecule screen identified cyclopiazonic acid (CPA) as a stressor to which stem cell-derived motor neurons were more sensitive than interneurons. CPA induced endoplasmic reticulum stress and the unfolded protein response. Furthermore, CPA resulted in an accelerated degeneration of motor neurons expressing human superoxide dismutase 1 (hSOD1) carrying the ALS-causing G93A mutation, compared to motor neurons expressing wild-type hSOD1. A secondary screen identified compounds that alleviated CPA-mediated motor neuron degeneration: three kinase inhibitors and tauroursodeoxycholic acid (TUDCA), a bile acid derivative. The neuroprotective effects of these compounds were validated in human stem cell-derived motor neurons carrying a mutated SOD1 allele ($hSOD1^{A4V}$). Moreover, we found that the administration of TUDCA in an $hSOD1^{G93A}$ mouse model of ALS reduced muscle denervation. Jointly, these results provide insights into the mechanisms contributing to the preferential susceptibility of ALS motor neurons, and they demonstrate the utility of stem cell-derived motor neurons for the discovery of new neuroprotective compounds.

INTRODUCTION

Amyotrophic lateral sclerosis (ALS) is a late-onset neurodegenerative disease that preferentially targets motor neurons in the cortex, brain stem, and spinal cord. Despite the discovery of >40 ALS-related genes,[1,2] the pathological processes leading to motor neuron degeneration and the reasons for differential neuronal subtype susceptibility to broadly expressed mutant proteins remain poorly understood. Even though many different cell types are involved in ALS pathogenesis,[3] cell-autonomous factors are believed to play a critical role during the early stages of the disease.[4–8]

Effective modeling of motor neuron degeneration is hindered by the limited accessibility of motor neurons in patients and animal models and by the fact that ALS is a late-onset disorder. The development of stem cell technologies that facilitate large-scale production of motor neurons carrying disease-causing mutations has circumvented the first challenge, and it has enabled biochemical analysis and drug screening in a relevant cellular context.[9–13] However, stem cell-derived motor neurons are transcriptionally and electrophysiologically immature, resembling embryonic or early post-natal motor neurons.[14–17] Most importantly, stem cell-derived motor neurons carrying ALS-causing mutations do not exhibit key hallmarks of motor neuron disease, such as aggregates of mutant proteins or p62-immunoreactive inclusions.[18–20]

Received 8 May 2018; accepted 16 October 2018;
https://doi.org/10.1016/j.ymthe.2018.10.010.

[7]These authors contributed equally to this work.

[8]Present address: Center for Neurodegenerative Disease Research, Department of Pathology and Laboratory Medicine, University of Pennsylvania, 3600 Spruce Street, Philadelphia, PA 19104, USA

[9]Present address: Department of Clinical Neuroscience, Division of Neurology, Karolinska Universitetssjukhuset, 171 76 Stockholm, Sweden.

[10]Present address: Novartis Institutes for BioMedical Research, Cambridge, MA 02139, USA.

[11]Present address: Biogen Inc., Cambridge, MA 02142, USA.

Correspondence: Hynek Wichterle, Departments of Neuroscience, Rehabilitation and Regenerative Medicine, and Neurology, Columbia University Irving Medical Center, 630 West 168th Street, New York, NY 10032, USA.
E-mail: hw350@cumc.columbia.edu
Correspondence: Sebastian Thams, Department of Clinical Neuroscience, Division of Neurology, Karolinska Universitetssjukhuset, 171 76 Stockholm, Sweden.
E-mail: sebastian.thams@ki.se

Despite their relatively immature state, several studies have reported differences in the survival, physiology, and biochemistry of cultured human and mouse stem cell-derived ALS motor neurons.[5,6,19,21–28] It has been suggested that many of these phenotypes result from a stressful *in vitro* environment that elicits premature or aberrant manifestations of pathological processes in cultured cells, yet the nature of these culture-related stressors remains ill defined. Understanding which specific stressors potentiate disease-relevant motor neuron pathology would enable the development of more faithful and reproducible models of ALS and, in turn, better tools to understand disease onset and progression. Ultimately, such models can be used to screen for neuroprotective drugs.

Here we describe the development of a highly sensitive motor neuron survival assay and how it was used to screen a library of bioactive compounds for stressors that accelerate the degeneration of mouse motor neurons carrying an ALS-causing human superoxide dismutase 1 (hSOD1)^{G93A} transgene.[29] The screen identified cyclopiazonic acid (CPA), an inhibitor of a calcium ATPase expressed in the endoplasmic reticulum (sarcoendoplasmic reticulum-associated calcium ATPase [SERCA]),[30] as a compound to which motor neurons are highly sensitive, particularly those expressing hSOD1^{G93A}.

In accordance with the literature, we demonstrate that CPA induces endoplasmic reticulum (ER) stress and activates the downstream cascades referred to as the unfolded protein response (UPR).[31] This cellular stress response is induced by unfolded and/or misfolded proteins in the ER lumen, and it is mediated by three ER sensors: IRE1α (Ern1), PERK (Eif2ak3), and ATF6. In turn, these sensors activate separate signaling cascades aiming to alleviate protein misfolding. Despite the initial adaptive response, prolonged activation of ER stress leads to the activation of apoptotic pathways and cell death.[32]

The accumulation of misfolded proteins is a hallmark of many neurodegenerative diseases, and it has been described in conjunction with the activation of ER stress in animal and stem cell-based models of ALS,[19,33–36] as well as in *post mortem* spinal cord samples from ALS patients.[33,37]

Studies in animal models of ALS show that certain motor neuron populations degenerate early during the course of the disease while others remain unaffected up until end stage.[38,39] Even though the underlying causes for this vulnerability are not fully understood, it was suggested that protein misfolding and ER stress in vulnerable motor neurons are early and crucial events that distinguish vulnerable from more resistant motor neurons.[34,40]

Based on our observation that CPA was selectively toxic to motor neurons, we developed an accelerated neurodegeneration assay, and we used it to screen for compounds that could attenuate the effects of ER stress. We demonstrate that kenpaullone, a protein kinase inhibitor that was recently shown to protect motor neurons from a neurotrophic factor withdrawal and to increase survival of human ALS motor neurons,[13,41] also protects motor neurons from ER stress. In addition to kenpaullone, we identified several other protective compounds, including additional kinase inhibitors and a bile acid derivative, tauroursodeoxycholic acid (TUDCA). In summary, we developed a novel, scalable, stem cell-based discovery platform that can be used for the evaluation of existing drugs and for the discovery of new compounds that protect motor neurons from ER stress-induced degeneration.

RESULTS

A Screen for Stressors Inducing Preferential Degeneration of Stem Cell-Derived hSOD1^{G93A} Motor Neurons

To gain insight into the cell-autonomous pathological mechanisms contributing to the onset of motor neuron degeneration in cells expressing mutant SOD1 protein, we developed a dual-color motor neuron survival *in vitro* assay. This robust, sensitive, and scalable system is ideal for the discovery of cell-autonomous motor neuron phenotypes.

To minimize well-to-well variation and to increase scalability, we designed an assay in which hSOD1^{WT} and hSOD1^{G93A} motor neurons (referred to hereafter as wild-type [WT] and ALS, respectively) expressing different fluorescent reporters were mixed in the same well (Figure 1A). For this purpose, we derived a set of new embryonic stem cell (ESC) lines by crossing mice carrying hSOD1^{WT} (WT control) or hSOD1^{G93A} (ALS mutant) transgenes[29] with mice expressing EGFP[12] or tagRFP under the control of a motor neuron-specific Hb9 (Mnx1) promoter (Figure S1A). Immunostaining with antibodies against Hb9 and the motor neuron transcription factor Islet1 confirmed that the new cell lines differentiated into motor neurons with comparable efficiency (Figures S1B–S1E), and immunoprecipitation confirmed the presence of misfolded SOD1 protein in mutant motor neurons (Figures S1F and S1G). RFP-expressing WT motor neurons were mixed with GFP-expressing ALS motor neurons in equal proportions, and they were cultured in 96-well plates (Figure 1A) in the presence of glial cell-derived neurotrophic factor (GDNF; G) and the cyclic AMP (cAMP)-elevating compounds IBMX (I) and forskolin (F).[42] Under these basal conditions, we observed a small decrease (~15%) in ALS motor neuron survival compared to WT controls (Figure S1H).

To identify stressors that potentiate ALS pathology, plated motor neurons were treated with a library of 1,275 biologically active small molecules (Tocris Screen Mini and Custom Collection, Tocris Bioscience). Compounds were added 24 hr after motor neuron plating at a final concentration of 10 μM using an automated robot-assisted liquid-handling platform. The ratio of surviving GFP (ALS):RFP (WT) motor neurons was determined 48 hr later, using whole-well imaging in conjunction with automated image analysis software (Figures S1I and S1J). The screen identified several compounds that preferentially decreased the survival of mutant motor neurons. These compounds included agonists and antagonists of membrane receptors, ion pump and channel inhibitors, an anti-mitotic drug, and general pro-apoptotic agents (Figures 1B and 1C).

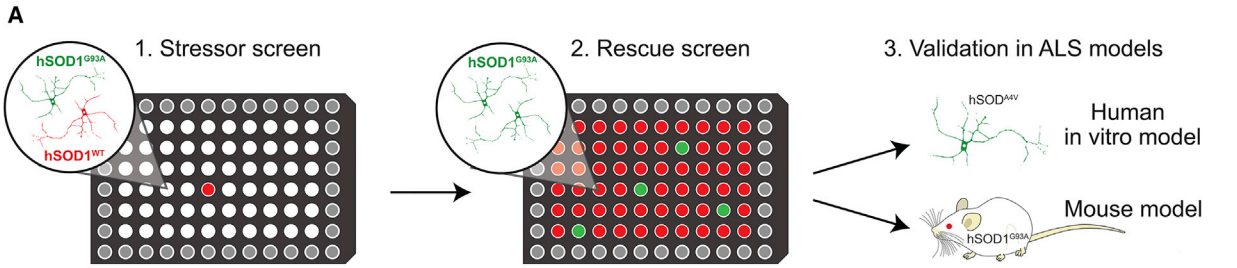

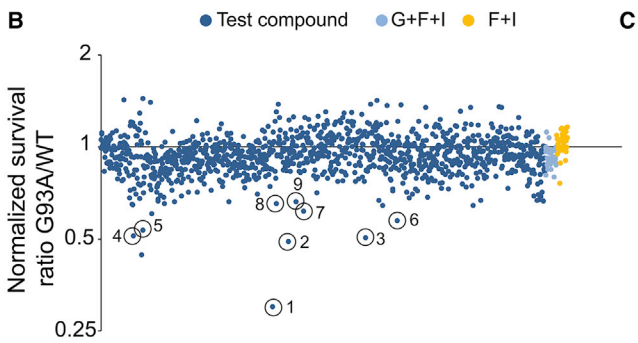

C

	Compound name	Ratio G93A/WT	Description
1	DH 97	0.301	MT2 receptor antagonist.
2	Monastrol	0.490	Selective inhibitor of mitotic kinesin Eg5.
3	Indirubin-3'-oxime	0.505	GSK3β inhibitor. Also inhibits other protein kinases.
4	(E)-Capsaicin	0.513	Prototypic vanilloid receptoragonist.
5	Dobutamine hydrochloride	0.536	α1, β1 and β2 receptor agonist.
6	2,3-DCPE hydrochloride	0.574	Selectively induces cancer cell apoptosis.
7	Fenretinide	0.618	Synthetic retinoid. Potent anti-cancer agent.
8	Cyclopiazonic Acid	0.655	Inhibitor of SERCA
9	U 99194 maleate	0.664	Potent,selectiveD3 antagonist.

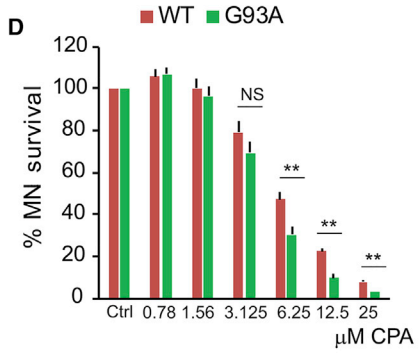

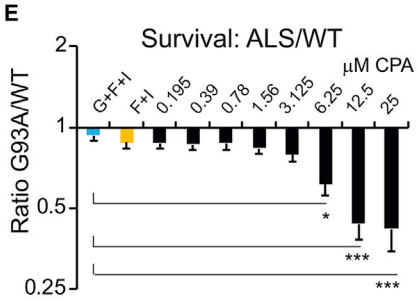

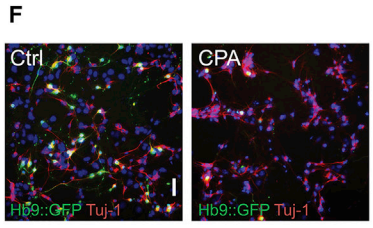

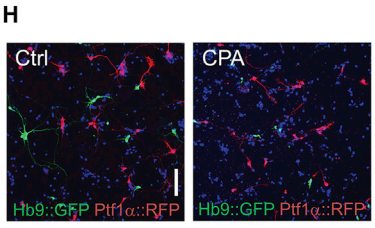

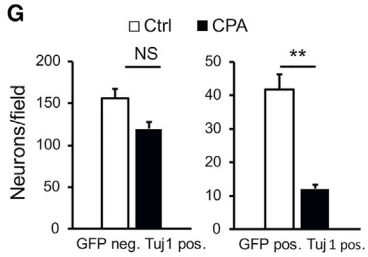

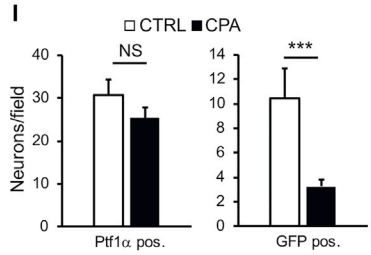

(legend on next page)

One of the selective stressors identified in the screen was CPA, a mycotoxin that reversibly blocks SERCA. SERCA is responsible for sequestering calcium from the cytoplasm into the ER.[30] Since calcium is an essential co-factor for protein-folding chaperones, SERCA blockade with subsequent depletion of calcium from the ER leads to the accumulation of misfolded proteins and activation of the UPR, ER stress, and apoptotic pathways.[31] We titrated CPA using two independent pairs of ALS-WT cell lines (Figures S2A and S2B) to establish the effective concentration range (6.25–12.5 μM; unless stated otherwise, all subsequent experiments were performed with 7.5 μM CPA) at which motor neurons show a reproducible cell death response. We found that ALS motor neurons exhibited reduced survival compared to WT motor neurons (Figures 1D and 1E).

To further investigate the effects of CPA, we examined whether it acts directly on motor neurons. We found that motor neurons purified by fluorescence-activated cell sorting (FACS) (Figures S2C–S2F) were as sensitive to CPA as motor neurons in mixed cultures, indicating that CPA acts directly on motor neurons rather than on other cell types that then produce secondary toxins.[5,6,8,43] These findings also suggest that the other cell types present in mixed cultures do not provide significant protection to CPA-treated motor neurons.

Preferential degeneration of motor neurons in the spinal cord, brain stem, and motor cortex is a hallmark of ALS.[44] To determine whether stem cell-derived motor neurons of spinal identity are more sensitive to CPA treatment than other spinal neurons, we immunostained surviving cells for pan-neuronal marker Tuj-1. Quantitative analysis of immunostained cultures revealed that, while the survival of GFP-expressing ALS motor neurons was reduced by ~71%, the survival of GFP^- $Tuj\text{-}1^+$ non-motor neurons of the same genotype was reduced only by ~23% (Figures 1F and 1G). The increased sensitivity of ALS motor neurons to CPA prompted us to ask whether even WT motor neurons are more sensitive to CPA than other nerve cells.

For this analysis, we generated a new ESC line that expresses tdTomato in dorsal spinal inhibitory interneurons derived from Ptf1α-expressing progenitors.[45] Following differentiation of this cell line under conditions that promote the specification of dorsal interneuron identity, tdTomato-expressing interneurons were co-cultured with GFP-expressing stem cell-derived motor neurons of spinal identity (Figures 1H and 1I). Quantification of RFP- versus GFP-positive neurons revealed that CPA treatment reduced dorsal spinal interneuron survival by only ~17%, compared to a ~70% decrease in the survival of co-cultured motor neurons. Together these data demonstrate that motor neurons expressing WT SOD1 too are significantly more sensitive to CPA than other spinal neurons of the same regional identity.

Effects of CPA on Cytosolic Calcium Levels

CPA is a reversible inhibitor of the SERCA pump, which is important for sequestration of cytosolic calcium into the ER. Indeed, CPA treatment resulted in an attenuated clearance of cytosolic calcium following motor neuron depolarization with kainic acid (Figures S3A–S3E). Elevated cytosolic calcium may activate multiple intracellular signaling processes, including cell death pathways.[46–48] Moreover, calcium dysregulation has been implicated in many neurodegenerative conditions, including ALS.[19,49–57] To determine whether motor neuron degeneration following CPA treatment is primarily caused by increased cytosolic calcium, we evaluated a panel of compounds with known effects on cytosolic calcium handling and/or signaling. These included BAPTA-am, a cell-permeable calcium chelator; dantrolene, an inhibitor of the ryanodine receptor that releases calcium from ER stores into the cytoplasm; three inhibitors of calpains, a family of calcium-dependent cysteine proteases; and three inhibitors of the calcium-activated kinase CaMKK/II. Notably, none of these treatments improved motor neuron degeneration or neurite retraction elicited by CPA exposure (Figures S4A and S4B). These data suggested that a cytosolic calcium overload is unlikely to be the primary cause of CPA-induced motor neuron death.

Stem Cell-Derived Motor Neurons Are Sensitive to the Activation of ER Stress Pathways

In addition to its effects on cytosolic calcium, CPA treatment has been shown to decrease calcium levels in the ER, leading to the activation of ER stress pathways.[31,58] These pathways are initiated by the binding immunoglobulin protein (BiP; HSPA5; GRP-78), an ER-resident chaperone, which translocates from its binding site on ER membrane-bound stress sensors upon detection of unfolded proteins in

Figure 1. Results from a Dual-Color Motor Neuron Stressor Screen: Dose-Respone Characterization of a Lead Compound and Subtype-Dependent Neuronal Survival

(A) Overview of the experimental design from primary stressor screen to secondary rescue screen and subsequent validation models. (B) Results of small molecule screen at 48 hr of exposure. Dark blue data points denote normalized G93A:WT survival ratio for well exposed to compounds, and light blue (negative control, GDNF + forskolin + IBMX + vehicle) and yellow data points (positive control, forskolin + IBMX + vehicle) denote G93A:WT survival ratio for the controls. (C) Circles mark confirmed lead compounds after secondary screening. (D and E) Dose-response curve (D) for cyclopiazonic acid (CPA), showing survival of Hb9::RFP $hSOD1^{WT}$ and Hb9::GFP $hSOD1^{G93A}$ motor neurons and normalized G93A:WT survival ratio (E). Results were compiled using two independent pairs of WT-G93A cell lines; individual results are shown in Figures S2A and S2B. Bars denote average, and error bars indicate SEM; $^*p < 0.05$, $^{**}p < 0.01$, and $^{***}p < 0.001$ (n = 9, one-way ANOVA, post hoc Dunnett's multiple comparison). (F and G) Light microscope micrographs (F) showing control and CPA-treated motor neuron cultures. Scale bar, 50 μm. Survival of ctrl and CPA-exposed $hSOD1^{G93A}$ GFP^+ motor neurons and $Tuj\text{-}1^+$ GFP^- neurons was quantified (G) at 48 hr (n = 3). (H and I) Light microscope micrographs (H) showing control and CPA-treated non-purified motor neuron-interneuron co-cultures. Survival of GFP^+ $hSOD1^{WT}$ motor neurons and $Ptf1\alpha^+$ interneurons was quantified (I) at 48 hr (n = 3). Scale bar, 50 μm. Survival of GFP^+ $hSOD1^{WT}$ motor neurons and $Ptf1\alpha^+$ interneurons was quantified at 48 hr (n = 3 for both analyses). Bars denote average, and error bars indicate SEM; $^{**}p < 0.01$ and $^{***}p < 0.001$ (n = 3, unpaired two-tailed Student's t test).

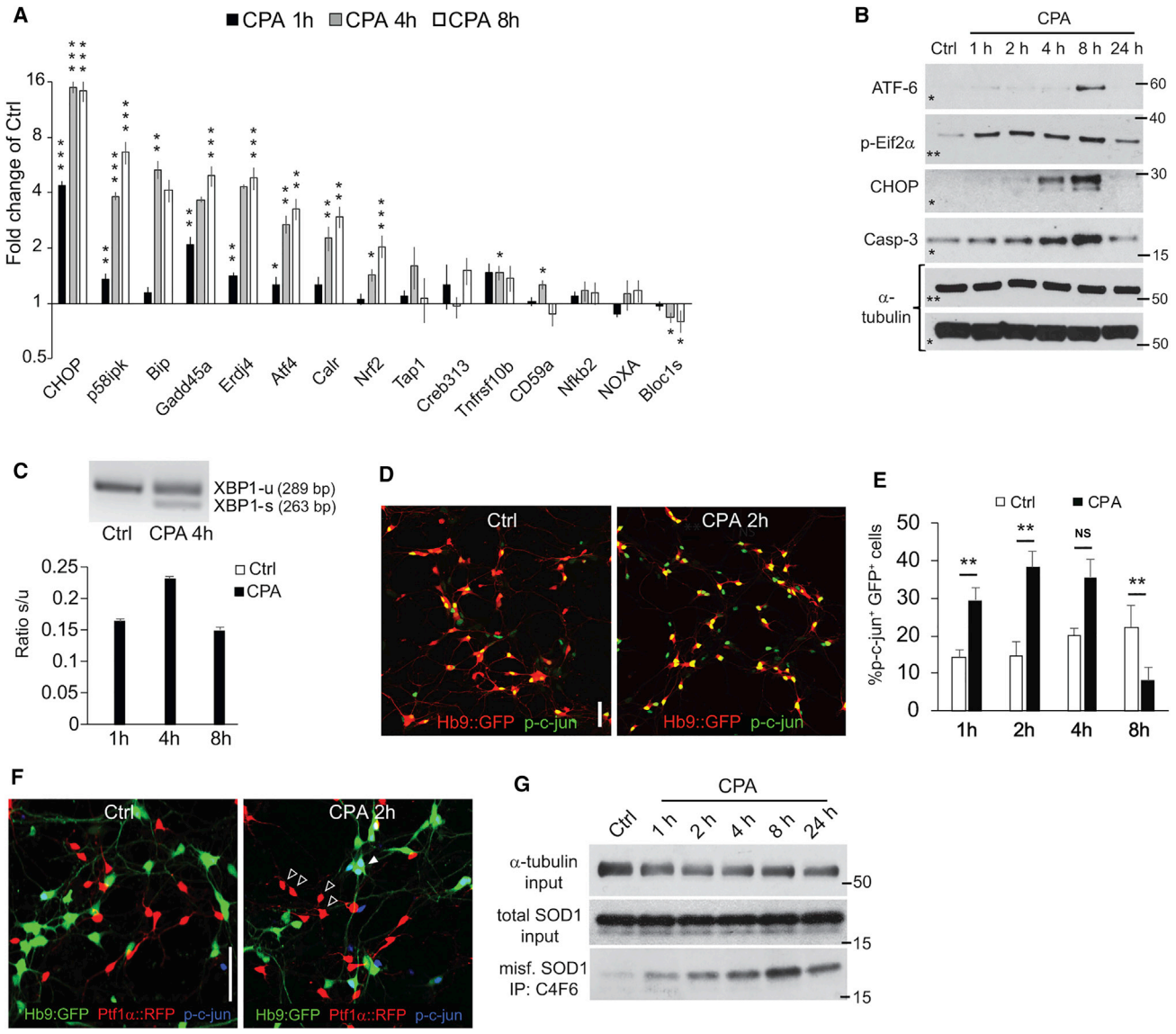

Figure 2. Characterization of ER Stress Markers in Motor Neuron Cultures Treated with Cyclopiazonic Acid

(A) Histogram showing qPCR results points to genes of particular interest at an earlier time after CPA exposure. RNA was extracted from unpurified hSOD1^{G93A} motor neurons (n = 3, independent culture dishes). Bars denote average, and error bars indicate SEM. CPA was compared to control for each gene and time point; *p < 0.05, **p < 0.01, and ***p < 0.001 (unpaired two-tailed Student's t test). (B) Immunoblots showing expression of ER stress-related proteins and their loading controls at different time points after CPA exposure (asterisks denote lanes originating from the same gel). (C) Histogram and inverted gel image showing XBP1 splicing in vehicle and CPA-treated hSOD1^{G93A} motor neurons at different time points after CPA exposure (n = 3). Bars denote average ratio s/u, and error bars indicate SEM. Note that no XBP1 splicing was detected in the vehicle-treated group (ctrl). (D and E) Confocal micrographs (D) and histograms (E) showing phospho-c-*jun*$^{+}$ motor neurons in ctrls and CPA-treated motor neuron cultures (n = 5). Scale bar, 50 μm. Bars denote average, and error bars indicate SEM; **p < 0.01 (one-way ANOVA, post hoc Dunnett's multiple comparison test). (F) Confocal micrograph showing phospho-c-*jun* staining (blue) in co-cultures of ALS motor neurons and dorsal interneurons (Ptf1α^{+}). Empty arrowheads indicate CPA-treated interneurons negative for phospho-c-*jun*, and filled arrowheads indicate motor neurons with strong nuclear staining for phospho-c-*jun*. Scale bar, 50 μm. (G) Immunoblots showing SOD1 expression and input loading control protein (α-tubulin) in lysates from CPA-treated hSOD1^{G93A} cells. Middle lanes show panSOD1 expression. Lower lanes show immunoprecipitated lysates using antibodies specific for misfolded hSOD1 species (C4F6 clone).

the ER lumen. Unbound BiP is involved in the activation of three separate signaling pathways associated with the UPR: the PERK, ATF-6, and IRE1α pathways.[59–62]

To assess the activation of these pathways in motor neurons exposed to CPA, we used RT-PCR to examine the expression levels of 15 stress-associated genes at three time points following CPA treatment

in hSOD1^{G93A} motor neurons (Figure 2A). We observed a rapid increase in the expression of *Bip* and the key downstream effector *Chop (Ddit3)*. *Bip* increased 2-fold after 1 hr of CPA exposure, and it continued to increase to approximately 5-fold by 8 hr. *Chop* was induced 4-fold after 1 hr of CPA treatment, and it reached 16-fold induction after 4 and 8 hr. Other genes with >2-fold induction included the following: *p58^{IPK}* (6.5-fold at 8 hr), an ER stress-induced protein kinase; *Growth arrest and DNA damage-inducible protein 45 alpha* (*Gadd45a*, 5-fold at 4 hr), which has been shown to be upregulated in the spinal cord of presymptomatic SOD1^{G93A} mice;[34] *Erdj4*, a Bip cofactor with involvement in ER-associated protein degradation (ERAD) (5-fold at 4–8 hr); *Atf4*, a downstream mediator of the PERK axis of the UPR (3-fold at 8 hr); *Calreticulin*, an ER-associated chaperone (3-fold at 8 hr), which was linked to nitric oxide (NO)-mediated motor neuron degeneration in hSOD1^{G93A} mice;[49] and *Nrf2*, a PERK substrate (2-fold at 8 hr). Taken together, these expression changes pointed to strong activation of multiple axes of the UPR in motor neurons exposed to CPA.

Western blot analysis of protein extracts from control and mutant motor neurons exposed to CPA for 1, 2, 4, 8, and 24 hr confirmed the early activation of the PERK pathway: an increase in Eif2α phosphorylation was already detectable after only 1 hr of CPA exposure, followed by the induction of CHOP (Figure 2B; Figures S6A–S6C). An accumulation of the active cleaved form of ATF-6 was detectable at 8 hr (Figure 2B). Activation of the IRE1α branch was assessed by qPCR analysis of *X-box-binding protein 1 (XBP1)* splicing, which was already induced by 1 hr of CPA treatment and persisted at 4 and 8 hr of exposure. Splicing of XBP1 was not detected in vehicle-treated controls (Figure 2C; Figure S6D). We further evaluated activation of the IRE1α branch by immunocytochemical analysis of c-*jun* phosphorylation,[63] which peaked after 2 hr of CPA treatment (Figures 2D and 2E). Notably, reactive c-*jun* phosphorylation was absent in Ptf1α-expressing interneurons exposed to CPA (Figure 2F). Finally, we detected increased levels of cleaved caspase-3 after CPA exposure, with a peak at 8 hr, indicating an apoptotic mechanism for cell death.

We considered the possibility that the effects of CPA treatment might reflect increased levels of the proximal disease trigger: accumulation of misfolded SOD1 protein in cultured motor neurons.[18,33,34,65,66] We treated mutant motor neurons with CPA or vehicle, and we immunoprecipitated misfolded SOD1 using two different conformation-specific hSOD1 antibodies. Western blot analysis revealed a CPA-dependent increase in the accumulation of misfolded SOD1 (Figure 2G; Figure S6E), potentially explaining the accelerated death-inducing effects of CPA in ALS motor neurons.

Compounds that Protect Motor Neurons from CPA-Induced Degeneration

The realization that motor neurons are more sensitive to the activation of ER stress pathways than other spinal neurons prompted us to set up a candidate molecule screen to identify compounds that increase motor neurons' resistance to CPA. Such compounds might alleviate neurodegeneration in ALS, as well as other conditions associated with protein misfolding and ER stress activation.[32] We screened a panel of >100 compounds that was compiled from in-house libraries and supplemented with compounds that emerged from a literature search (Table S1). Compounds in the panel are known to modulate different branches of the UPR, influence calcium sequestration, act as neurotrophic factors, and/or promote motor neuron survival.

hSOD1^{G93A} motor neuron cultures were treated with rescue compounds for 45 min prior to the addition of 7.5 μM CPA. Survival and neurite growth were assessed after 24 and 48 hr. The screen yielded several compounds that prevented more than 50% of motor neuron degeneration in response to CPA (Figure S4A): the c-Jun N-terminal kinase (JNK) inhibitor SP600125; the tyrosine kinase inhibitor sunitinib; and the broad-spectrum kinase inhibitors Ro 31-8220 mesylate, kenpaullone, GÖ6976, H-7, and K252a.[67–69] Compounds that rescued over 50% of neurite growth included the neurotrophic factor Cardiotrophin-1; the p38 inhibitors SB293063 and SB203580; SP600125; the bile acids taurine-conjugated cholic acid (TCA), taurine-glycine-conjugated cholic acid (TGCA), and TUDCA; and the kinase inhibitors Ro 31-8220 mesylate, GÖ6976, sunitinib, kenpaullone, H-7, and K252a (Figure S4B). Overall, GÖ6976, kenpaullone, K252a, and TUDCA appeared to be the most promising candidates (Figure 3A), due to their strong survival-promoting effects at low concentrations (GÖ6976, kenpaullone, K252a) or strong neurite outgrowth-promoting effects (TUDCA).

By testing the ER stress gene panel presented in Figure 2A in cultures treated with CPA and rescue compounds, we confirmed that two of the protein kinase inhibitors, GÖ6976 and kenpaullone, attenuated the cell stress-signaling cascade at different levels (Figures S7A and S7B).

Furthermore, GÖ6976 and K252a treatments suppressed c-*jun* phosphorylation in CPA-exposed cultures more effectively than kenpaullone (Figures 3B and 3C), indicating that the latter inhibitor acts, at least in part, on a different target pathway (Figure 3D). TUDCA, an ambiphilic bile acid component that functions as a chemical chaperone, rescued neurite outgrowth (Figure 4A), but it only showed a moderate effect on motor neuron survival and failed to suppress c-*jun* phosphorylation (Figures 3B and 3C; Figure S4A). TUDCA, which can be expected to act at the protein level, did not result in any major changes in the expression of ER stress-related genes, as shown by selected results from an RNA sequence screen (Figure S7C).

Validating Protective Compounds in Human Stem Cell-Derived Motor Neurons

To adapt the assay to human cells, we generated a new isogenic pair of ESC lines derived from a human ESC line expressing GFP under the control of the Hb9 motor neuron promoter (HUES3 *HB9*::GFP[5]). The ALS-causing A4V mutation was introduced into a single allele of the human *SOD1* gene using zinc-finger nuclease (ZFN)-based genome engineering to recapitulate human patient genotypes (Figures S5A–

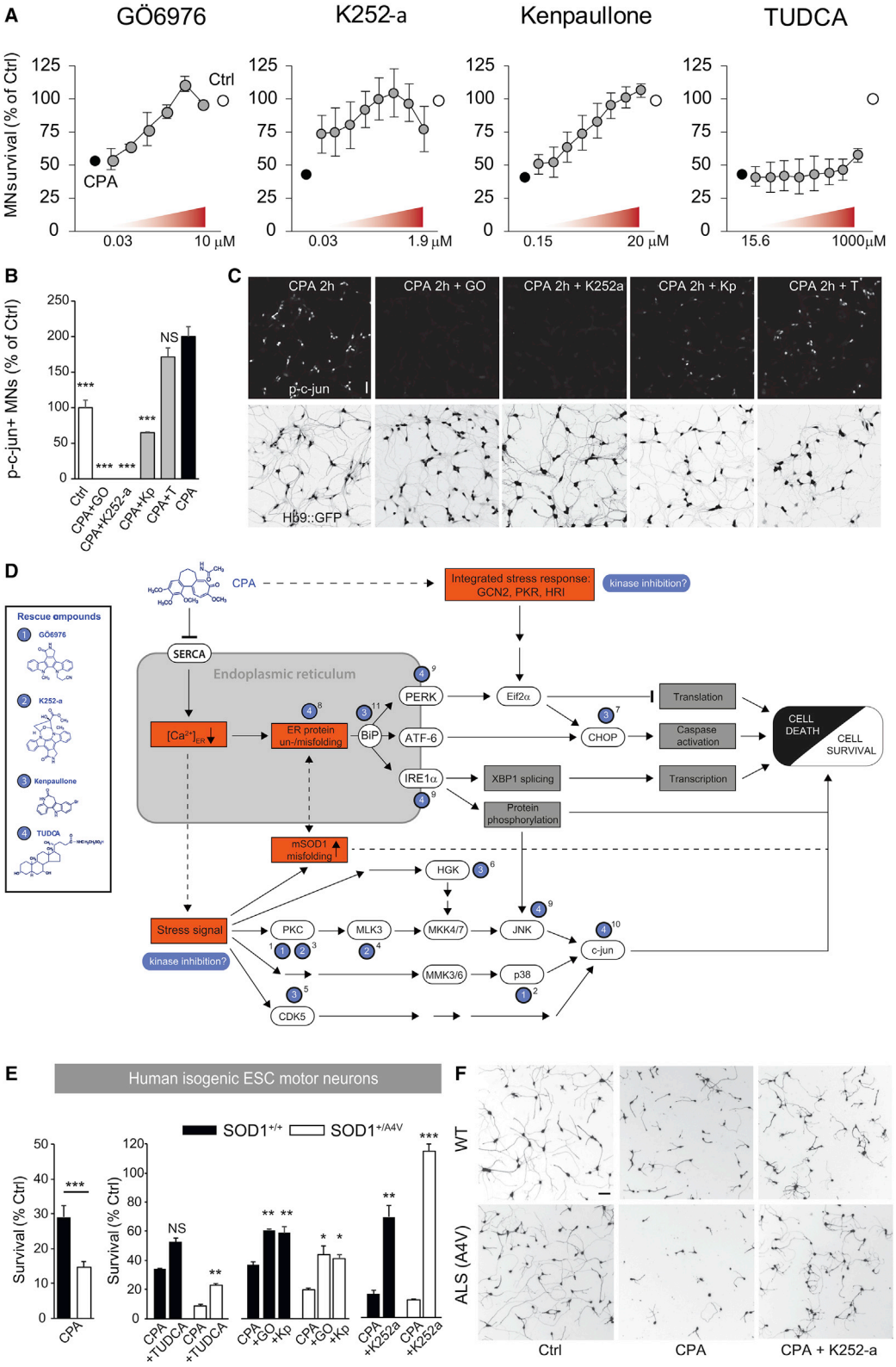

(legend on next page)

S5C). The pair of cell lines was differentiated into motor neurons using previously published protocols;[9,70] their relative susceptibility to ER stress-mediated neurodegeneration was assessed under increasing concentrations of CPA. While human motor neurons were less sensitive to CPA than mouse motor neurons (Figure S5K), we detected a significantly increased sensitivity of mutant human SOD1^{A4V} motor neurons exposed to 33 μM CPA (~14% survival) compared to control neurons (~29% survival) (Figure 3E), thereby recapitulating the genotype-dependent effects of CPA in mouse motor neurons.

Next, we used the assay to test whether compounds protective to mouse motor neurons would be also able to protect human motor neurons exposed to 33 μM CPA. Remarkably, all of the top protective compounds identified in the mouse motor neuron screen were also effective in protecting human motor neurons against CPA (Figure 3E). Pretreatment of human motor neurons with kenpaullone rescued 35% of CPA-induced cell death in WT motor neurons and 26% in SOD1$^{+/A4V}$ motor neurons (Figure 3E), but it had no significant effects on neurite growth (Figure S5L). GÖ6976 rescued 35% of cell death in hSOD1$^{+/+}$ motor neurons and 30% in SOD1$^{+/A4V}$ motor neurons (Figure 3E), and it also significantly rescued the decrease in neurite outgrowth (Figure S5L). K252a was overall the most promising compound, rescuing 63% of cell death in hSOD1$^{+/+}$ and 100% of cell death in hSOD1$^{+/A4V}$ motor neurons (Figures 3E and 3F), with significant effects on neurite growth for both genotypes (Figure S5L). Finally, TUDCA reduced cell death moderately in hSOD1$^{+/+}$ and hSOD1$^{+/A4V}$ motor neurons by 29% and 15%, respectively, with a small significant effect on neurite growth only in hSOD1$^{+/A4V}$ motor neurons (Figure 3E; Figure S5L).

TUDCA Treatment Attenuates ALS-Associated Muscle Denervation *In Vivo*

TUDCA is a dietary supplement, and its effects on diverse pathological conditions have been the focus of multiple clinical trials (GEO: NCT00877604, NCT02218619, NCT00771901, and NCT01829698; [71]). TUDCA is generally safe, has very few side effects, and exhibits good blood-brain barrier penetrance when administered subcutaneously or orally.[71,72] Denervation of neuromuscular junctions (NMJs) is one of the earliest phenotypes observed in mouse models of ALS,[73–76] and, in the light of the *in vitro* results, we reasoned that TUDCA might promote the maintenance of motor axon terminal integrity and delay the denervation process.

To compare the effectiveness of TUDCA to its analogs, we screened it in parallel with 10 conjugated bile acids in CPA-treated motor neurons. TGCA matched the moderate effects of TUDCA on motor neuron survival, and it worked at lower concentrations; however, it had smaller effects than TUDCA on neurite extension (Figures S4C and S4D). TCA exhibited similar effects to TUDCA on both motor neuron survival and neurite extension, but it did not offer any advantages in terms of drug development. Thus, we decided to proceed with TUDCA for further evaluation *in vivo*.

To test the ability of TUDCA to preserve motor axons in ALS models *in vivo*, we designed a small-scale study in which we evaluated the denervation of the fast fatigable hind limb muscle *tibialis anterior* (TA) in early disease-stage hSOD1^{G93A} ALS mice (Figure 4C). We have previously determined that TA motor neurons in fast-progressing hSOD1^{G93A} ALS mice undergo a period of presymptomatic events, including ER stress, beginning at post-natal day (P)30, followed by muscle denervation that extends to P50.[40] During this period, the TA muscles display 25%–40% denervation before becoming substantially atrophied at later time points. To target this window of early cell stress events,[34] we treated hSOD1^{G93A} mice with subcutaneous TUDCA or vehicle injections every 3 days between P30 and P50. Mice expressing mouse WT SOD1 were treated only with TUDCA, and they served as reference for the analysis. At the end of the experiment, we counted total NMJs by staining for acetylcholine receptors in the TA muscles with Alexa Fluor 555-conjugated α-bungarotoxin, and we assessed their innervation by staining for motor axons with antibodies against vesicular acetylcholine transferase (VAChT) (Figures 4D and 4E). Despite the fact that the mice received only seven injections over the course of 21 days of treatment, we observed a moderate, but statistically significant increase in NMJ innervation in TUDCA-treated hSOD1^{G93A} mice compared to vehicle-treated animals (Figure 4D).

DISCUSSION

In this study, we used a novel stem cell-based discovery platform to detect compounds rescuing human and mouse motor neurons from

Figure 3. Characterization of Rescue Compounds, Including Their Effects on c-*jun* Phosphorylation in Mouse Motor Neurons and Survival in Human Motor Neurons

(A) Dose-reponse curves for the lead compounds from the rescue screen (GÖ6976, n = 6 culture wells; K252a, n = 2 independent cultures; kenpaullone, n = 3 independent cultures; and TUDCA, n = 2 independent cultures). Bars denote average, and error bars indicate SEM. (B and C) Histogram (B) and confocal micrographs (C), showing the effects of rescue compounds on phospho-c-*jun* expression in CPA-treated motor neuron cultures at 2 hr of exposure. Bars denote average, and error bars indicate SEM; all groups were compared to CPA, ***p < 0.001 (one-way ANOVA, post hoc Dunnett's multiple comparison test). Scale bar, 50 μm. (D) Proposed model for putative signaling pathways for CPA and targets for rescue compounds. Blue numbered labels indicate reported upstream or direct effects for the different rescue compounds. Intact lines show reported signaling pathways, and dashed lines show suggested pathways. Abbreviations are as follows: General control non-depressible 2, GCN2; Protein kinase R, PKR; and Heme-regulated inhibitor, HRI. Superscript numbers denote supporting references as follows: 1, Sakaki et al.[67]; 2, Lemonnier et al.[85]; 3, Kase et al.[68]; 4, Roux et al.[69]; 5, Sun et al.[86]; 6, Yang et al.[13]; 7, Meares et al.[79]; 8, Uppala et al.[93]; 9, Özcan et al.[92]; 10, Castro-Caldas et al.[91]; 11, present study. (E) Histogram showing the effects of CPA and in the absence or presence of rescue compounds (GO, GÖ6967; Kp, kenpaullone) in FACS-purified Hb9::GFP^{+} human motor neurons differentiated from an SOD1$^{+/+}$ and an isogenic genetically modified SOD1$^{+/A4V}$ human ESC (hESC) line (n = 9 for CPA versus CTRL for both genotypes, and n = 3 for all rescue compounds for both genotypes). Bars denote average, and error bars indicate SEM; *p < 0.05, **p < 0.01, and ***p < 0.001 (unpaired two-tailed Student's t test). (F) Representative cropped whole-well images showing calcein^{+} motor neurons. Scale bar, 50 μm.

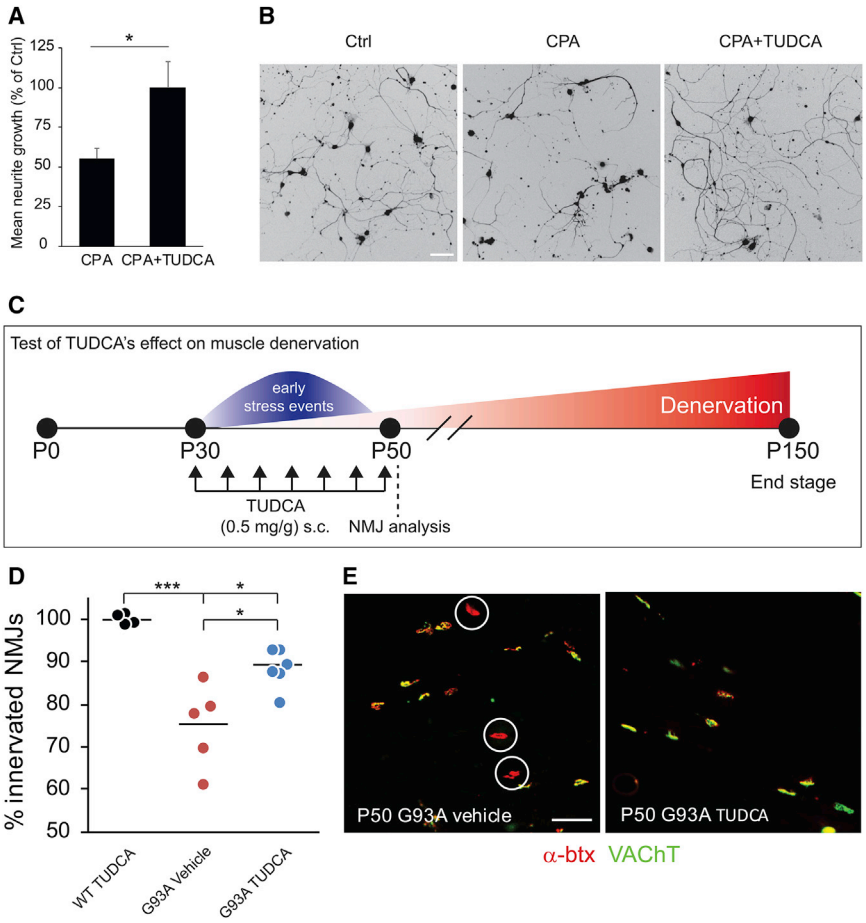

Figure 4. Characterization of TUDCA's Effects *In Vitro* and on Muscle Denervation *In Vivo* in a Mouse Model of ALS

(A) Histogram showing rescue effects of TUDCA on CPA-induced neurite degeneration. Bars denote average, and error bars indicate SEM; *p < 0.05 (unpaired two-tailed Student's t test). (B) Representative light microscope micrographs showing the effects of TUDCA application in cultures exposed to CPA. Scale bar, 50 μm. (C) Experimental design for the *in vivo* test of TUDCA on muscle denervation in hSOD1^{G93A} mice. (D) Scatterplot showing NMJ innervation in the TA (n = 4 for WT + TUDCA, n = 6 for G93A + TUDCA, and n = 5 for G93A + vehicle). Data points represent individual animals, and horizontal lines denote the average; *p < 0.05 and ***p < 0.001 (one-way ANOVA, post hoc Dunnett's multiple comparison test). (E) Confocal micrographs showing images from TA NMJs (α-btx, red; VAChT, green) of vehicle and TUDCA-treated hSOD1^{G93A} mice. Circles denote denervated NMJs. Scale bar, 50 μm.

a biological stressor, CPA, which mimics important aspects of neurodegeneration. To streamline future drug discovery, we used this platform to design a translational pipeline, in which lead compounds identified through screening can be readily evaluated in both human cells and via a short-term assay in presymptomatic ALS mice.

Modeling degenerative diseases in cell culture systems opens new opportunities to investigate the pathological processes associated with disease-causing mutations and to screen for novel therapeutic agents. However, adult-onset degenerative diseases, where causative mutations result in relatively slow but accumulating cellular insults, are difficult to model in the kinds of short-term culture systems that are compatible with high-throughput drug screening. We reasoned that the discovery of stressors that induce and accelerate phenotypic changes in motor neurons *in vitro* could provide insights into molecular pathways contributing to motor neuron degeneration and could lead to the discovery of motor neuron-protective compounds.

ALS-causing mutations are not overtly toxic to spinal motor neurons, and, accordingly, patients do not show any obvious motor deficits during the presymptomatic phase of the disease. Even in an aggressive mouse model of ALS caused by overexpression of mutant hSOD1, no motor neuron death is observed until adulthood,[77] indicating that the effects of ALS mutations are either cumulative or that they are potentiated by age- and/or environment-related stressors. To identify stressors that contribute to the degeneration of motor neurons, we designed a highly sensitive, intrinsically controlled survival assay. The co-culture setup allowed us to focus on the intrinsic properties of motor neurons expressing disease-causing mutant SOD1 protein that may render them more sensitive to stressors than WT cells. Using this platform, we identified CPA as a compound that is selectively toxic to motor neurons in general, with further accentuated effects in cells expressing mutant SOD1.

The role of ER stress in ALS remains controversial. While signs of ER stress have been detected in both mouse models of the disease[34,40,64] as well as in *post mortem* ALS patient spinal cords, several studies have suggested that the induction of ER stress pathways might be a protective response, facilitating the clearance of ALS-causing mutant proteins.[78] Interestingly, instead of improved clearance, we observed an accumulation of misfolded SOD1 protein following ER stress induction. This finding raises the possibility that, under basal conditions, young motor neurons are capable of effectively clearing misfolded SOD1. However, as the burden of misfolded proteins increases with time, the clearance mechanisms may become overwhelmed, resulting in less effective removal of mutant SOD1. It is tempting to speculate that CPA effectively mimics the age-related increase in endogenous protein misfolding at a dramatically accelerated pace.[35]

Interestingly, our model recapitulates another poorly understood but important feature of ALS. We observed that motor neurons were

considerably more sensitive to ER stress-inducing compounds than other types of neurons. While we do not know what mechanisms underlie such cell type-specific sensitivity to ER stress, it might explain the preferential degeneration of spinal motor neurons in familial cases of ALS, despite broad expression of misfolded proteins in all types of neurons.

A screen of candidate neuroactive compounds identified several potent drugs that could reverse the harmful effects of CPA. Two classes of compounds were of particular interest: kinase inhibitors and bile acid derivatives. Kinase inhibitors exhibited a remarkable ability to protect motor neurons from CPA toxicity. One compound, kenpaullone, was previously shown to protect motor neurons from neurotrophic deprivation,[13] improve survival, reverse electrophysiological deficits in human stem cell-derived motor neurons from a patient carrying a mutation in the *FUS* gene,[41] and decrease the levels of the UPR mediator CHOP in neural cells exposed to the ER stressor tunicamycin.[79] In addition to kenpaullone, we identified two staurosporine analogs, K252a and GÖ6976, that were previously reported to increase neuronal survival in other *in vitro* models of neurodegeneration.[69,80]

By integrating our results with published studies, we propose a model in which CPA induces a stress response that activates a cascade of intracellular protein kinase-regulated pathways,[81,82] including a protein kinase C (PKC)-JNK-signaling pathway[67,68] (Figure 3D). GÖ6976 and K252a strongly inhibit PKC, as well as its downstream target mixed lineage kinase 3 (MLK3).[69] Kenpaullone acts primarily as an inhibitor of HPK1/GCK-like kinase (HGK)[13] and cyclin-dependent kinases (CDKs).[83,84] Due to the unselective nature of these compounds, additional stress-activated kinase pathways may be involved, such as p38.[85,86] Consequently, we did not discern a consistent pattern that would point to a common upstream target mechanism. Our conclusion is that the kinase targets differ between the compounds and act on different branches of the same cell stress-induced cascade, ultimately converging on the suppression of c-*jun* phosphorylation (Figure 3D).

Testing these kinase inhibitors *in vivo* will require further optimization of their pharmacokinetic and pharmacodynamics properties. Kenpaullone is insoluble in aqueous solutions at its most effective concentrations, effectively preventing its testing *in vivo*. While K252a and GÖ6976 are more potent and more soluble than kenpaullone (data not shown), these compounds are broad-spectrum inhibitors, each targeting >100 different kinases, raising the concern of adverse secondary effects *in vivo*. Future drug development and mechanistic target studies will, therefore, require the design of more selective inhibitors.

The second class of neuroprotective compounds that emerged from our screen was derivatives of mammalian bile acids, which have been used extensively in traditional Tibetan and Chinese medicine. Notably, it shows potentially beneficial results in ALS patients.[71] While this class of compounds protected <30% of dying motor neurons after CPA exposure, it completely restored neurite outgrowth. In contrast to the kinase inhibitors that are not approved for human use, TUDCA is a widely available dietary supplement, and its analog UDCA is a water-soluble FDA-approved drug for treating pruritus and liver disease. TUDCA has previously been shown to have beneficial effects in mouse models of Huntington's, Parkinson's, and Alzheimer's diseases.[87–91] TUDCA has also been shown to reduce the expression of markers of the UPR in a mouse model of type 2 diabetes, in part by acting as a chaperone for misfolded proteins[92,93] (Figure 3F). We therefore wanted to validate our results in an *in vivo* model, and we tested whether treatment with TUDCA was sufficient to delay muscle denervation in early-stage ALS mice. A brief treatment period showed an encouraging effect on denervation in the TA muscle, raising the possibility that TUDCA alone or in combination with other treatments might delay motor disease onset or progression.

In conclusion, the dual-color motor neuron-screening approach described herein revealed that stem cell-derived motor neurons are selectively sensitive to ER stress pathway activation. Our findings add to the mounting evidence that ER stress contributes to motor neuron cell death in ALS. The scalable stem cell-based screening system identified several compounds that effectively desensitize motor neurons to ER stress, providing new tool compounds for mapping pathways involved in motor neuron degeneration and for the development of analogs compatible with *in vivo* testing. This system can be easily adapted to other neurodegenerative conditions associated with ER stress activation, such as Parkinson's disease, Huntington's disease, prion disease, or Alzheimer's disease.[32]

MATERIALS AND METHODS

Derivation of Mouse Transgenic ESC Lines

Heterozygous Tg(Hlxb9-GFP)1Tmj or Tg(Hlxb9-tagRFP) reporter mice were crossed with mice expressing a mutated (B6.Cg-Tg(SOD1*G93A)1Gur/J) or WT form (B6SJL-Tg(SOD1)2Gur/J) of human SOD1. Blastocysts were collected at embryonic day 3.5. Mouse ESC lines were derived as previously described.[12] New lines were genotyped and sequenced to confirm the presence of both transgenes and the G93A point mutation.

For interneuron differentiations, mouse ESC lines were derived from *Ptf1α::cre* mice (kindly provided by Dr. Kaltschmidt) crossed to *Rosa-LSL-tdTomato* fluorescent reporter mice.[94,95] All animal work was performed in compliance with Columbia University Institutional Animal Care and Use Committee (IACUC) protocols.

Generation of Isogenic Human ESC Lines by Genetic Targeting

To extrapolate results from the mouse assays, we generated an independent set of $SOD1^{+/A4V}$ and $SOD1^{+/+}$ isogenic cell lines by introducing the A4V mutation into the WT SOD1 locus of the human ESC line HUES3 Hb9::GFP[5] (Figure S5). Using again a two-step nuclease-mediated gene-targeting strategy,[96] we introduced the SOD1A4V mutation into the HUES3 Hb9::GFP genetic background (Figure S5A).

Mouse and Human Differentiation into Spinal Neuronal Lineages

Motor neuron differentiation of transgenic mouse ESCs was performed as previously described.[12] Briefly, cells were dissociated on day 6 of differentiation and plated on a surface coated with poly-ornithine (Sigma, 100 μg/mL) and laminin (4 μg/mL). Cells were cultured in the presence of the cAMP-elevating compounds forskolin (10 μM) and IBMX (100 μM) in combination with 500 μM GDNF. For the majority of all experiments, mouse cultures containing motor neurons, interneurons, and glial progenitors were used (referred to as motor neuron cultures); in a few experiments, motor neurons were purified by FACS (see the Supplemental Materials and Methods).

For differentiation into dI4 interneurons, Ptf1α-tdTomato ESCs were dissociated and cultured in suspension as embryoid bodies (EBs) at a density of 8.0×10^5 cells/10-cm culture-treated Petri dish. On day 2 of differentiation, EBs were collected, spun down, and split 1:4 into new Petri dishes and supplemented with 1 μM retinoic acid (RA). Media were exchanged on days 4 and 6 of differentiation. The endpoint of dI4 interneuron (IN) differentiation was day 8, when EBs were collected for co-culture studies.

Differentiation of human isogenic HUES3 ESC HB9::GFP reporter lines into motor neurons was performed as previously described.[70] Cells were dissociated on day 16 of differentiation, sorted via FACS, and plated on poly-ornithine- and laminin-coated surfaces as above. Serum-free human motor neuron plating media were supplemented with the antimitotic UFdU and the neurotrophic factors GDNF, brain-derived neurotrophic factor (BDNF), ciliary neurotrophic factor (CNTF), and insulin-like growth factor 1 (IGF1) (all at 10 ng/mL) as described.[97]

All cell lines used were routinely tested for mycoplasma.

Dual-Color Motor Neuron Co-culture Assay

Dissociated fluorescent Hb9::RFP-hSOD1^{WT} cells were counted by hemacytometer and mixed with an equal number of Hb9::GFP-hSOD1^{G93A} motor neurons, such that 500 fluorescent cells of each genotype were plated per well. Cells were plated in coated 96-well plates in a medium containing FSK and IBMX (low trophic support, positive control for cell death) or FSK, IBMX, and 250 pg/mL GDNF (medium trophic support, positive control for survival).

Automated Image Analysis

Whole-well images of live GFP$^+$ cells were acquired using a Plate Runner^{HD} system (Trophos). Images were analyzed using Metamorph software (Molecular Devices). A healthy cell criterion, i.e., neurons with a significant neurite (5× cell body diameter), was used to distinguish live neurons from GFP$^+$ debris (Figure S1K). The endogenous Hb9::GFP reporters in the human lines were not bright enough to be faithfully detected on our automated imaging platform. Cells were treated immediately prior to imaging with the live-cell dye calcein-AM (1.33 μM) for 10 min, followed by quenching with a 10% solution of hemoglobin in PBS.

Small Molecule Screen

Approximately 1,300 biologically active compounds from the Tocris Mini Screen and Custom collection were added to screening plates at a final concentration of 10 μM in singletons. The final concentration of DMSO was 0.5%. A survival ratio was calculated by dividing the number of surviving GFP$^+$ cells by the number of RFP$^+$ cells after 48 hr of exposure to the compounds.

FACS

Cells were sorted based on GFP or RFP expression using a 5-laser ARIA-IIu ROU Cell Sorter (BD BioSciences) configured with a 100-μm ceramic nozzle and operating at 20 psi.

ER Stress Rescue Screen

Dissociated and plated cells were allowed to recover for 24 hr, following 45-min incubation with rescue compounds or medium + 0.5% DMSO as control. Compounds were screened in triplicates at three different concentrations with 5-fold dilution steps; hits were further evaluated in 6- to 8-point serial dilutions in 3–6 replicates. Rescue compounds were selected from the initial dual-color screen or from a literature search focusing on compounds with documented effects on ER stress in other models. Cells were then exposed to 7.5 μM CPA for mouse cells and 33 μM for human cells or medium + vehicle 0.5% DMSO, which we referred to as control (ctrl) throughout.

Immunocytochemistry

Live cultures were pre-fixed with 4% paraformaldehyde (PFA) on ice, by adding fixative directly to the medium for 2 min, then fixed an additional 15 min by replacing the well content with 4% PFA and incubating at 4°C. Fixed cultures were blocked for 1 hr at room temperature with 0.01 M PBS containing 0.3% Triton-X and 20% donkey serum. Primary antibodies were diluted in blocking solution and incubated overnight at 4°C, followed by incubation with secondary antibodies (Alexa donkey 488/555/647) for 60 min at room temperature.

Biochemistry

Day 6 EBs were lysed in TNG-T lysis buffer[65] containing protease (Complete Mini) and phosphatase (PhoStop) inhibitors for 30 min, followed by mechanical trituration with a 26G syringe. C4F6 and B8H10 antibodies (MediMabs) were coupled to protein-G Dynabeads and used for the immunoprecipitation of misfolded hSOD1, as described.[65] A control immunoglobulin G (IgG) antibody was used a negative control (Figure S1I). A pan-SOD1 antibody (Novus Biologicals) was used for immunoblotting; 5% of the input was used as a loading control. For western blotting, the following antibodies were used: Caspase-3 (1:1,000), CHOP (1:500), phospho-Eif2α (1:1,000) (Cell Signaling Technology), SOD1 and ATF-6 (1:200, Novus Biologicals), and α-tubulin (1:50,000, Abcam). Representative gels are cropped from scanned images of the original films. Cropped parts without relevance to the present study are indicated by a dashed line in the figure.

qPCR

Cultures were treated with vehicle or CPA, and samples were collected at 1, 4, and 8 hr. In addition, the combinations CPA + kenpaullone and CPA + GÖ6976 were evaluated at 4 and 8 hr. Samples were lysed in TRIzol and frozen at −80°C until further processing. RNA was extracted using the Qiashredder and QIAGEN RNeasy Mini kits (QIAGEN), according to the manufacturer's protocol. 1–2 μg total RNA was used for each reverse transcription reaction, and reactions were performed using the TaqMan RT kit (Applied Biosystems, Grand Island, NY, USA). Primer pairs were designed for target transcripts using Primer Express 3.0 (Applied Biosystems). qPCR reactions were performed using the Power SYBR Green PCR Master Mix (Applied Biosystems). Reactions were run and analyzed on a ViiA 7 (Life Technologies) qPCR instrument using absolute quantification settings. Statistics were performed using delta-CT values, and data were visualized using fold change values.

XBP1 Splicing

PCR was performed in a 50-μL jumpstart Taq (Sigma-Aldrich, D9307) reaction containing 10 pmol XBP-1-specific primers to detect splicing (forward: 5′-GAATGCCCAAAAGGATATCAGACTC-3′, reverse: 5′-GGCCTTGTGGTTGAGAACCAGGAG-3′). PCR conditions were as follows: 1 cycle of 94°C for 1 min; 30 cycles of 94°C for 30 s, 60°C for 30 s, and 72°C for 1 min; and one cycle of 1 min at 72°C. PCR products were run for 30 min on 2.5% agarose gels containing ethidium bromide. Bands were observed and quantified using the Syngene G:Box and Genesis software. Band intensity was measured using the *Analyze-Gels* application in ImageJ (NIH).

Calcium Imaging

Hb9::RFP WT and ALS motor neurons were dissociated on day 6 of differentiation, and they were cultured 3 days on glass coverslips. The coverslips were incubated with 5 μM Fura-2 AM, ratiometric calcium indicator dye (Life Sciences, USA), for 30 min at room temperature. Coverslips were then exposed to a 1-s pulse of 100 μM kainic acid (KA), and one image per second was acquired for 1 min. After a recovery period of 2 min, the coverslips were then continuously exposed to 75 μM CPA for 20 min, and one image was acquired every 30 s. After another 2-min recovery period, a second pulse of KA was applied, with the same image acquisition as the first application. A 340:380 ratio was calculated for all image series using FIJI (http://fiji.sc/). Quantification was carried out using Igor Pro version (v.)6 (Wavemetrics, USA). The rate at which the evoked calcium transients returned to the baseline was calculated from the tau (time constant) of a single exponential curve fitted to the falling part of the Ca intensity trace from 80% to 20% of the peak.

In Vivo Administration of TUDCA

P30 mice were divided into three cohorts:[1] hSOD1^{G93A} mice (B6.Cg-Tg(SOD1*G93A)1Gur/J) receiving 0.5 mg/g TUDCA in 0.01 M PBS subcutaneously;[2] WT mice (C57BL/6J) receiving 0.5 mg/g TUDCA in 0.01 M PBS subcutaneously, to evaluate the mutation-specific effects of NMJ denervation and of the drug; and[3] hSOD1^{G93A} mice receiving 0.01 M PBS subcutaneously, as a vehicle control. The drug was administered every 3 days from P30 to P51 for a total of 7 injections, after with animals were euthanized. The TA muscles were dissected out and processed for staining, following transcardiac perfusion. Presynaptic terminals were stained with an antibody to VAChT (raised in rabbit, Covance, 1:32,000), and postsynaptic clusters were stained with α-bungarotoxin conjugated to Alexa Fluor 488 (1:500; Invitrogen). NMJs lacking presynaptic staining were considered denervated. Every third section throughout the whole muscle was analyzed from one TA per animal (n = 4–6). All animal work was performed in compliance with Columbia University IACUC protocols.

Statistics

Statistical analyses were performed with GraphPad Prism v.7 or R' (www.r-project.org). Datasets are expressed as mean value ± SEM throughout the paper. If normal distribution and equal variance could be assumed, analysis of significance was performed with an unpaired two-tailed Student's t test for pairwise comparison or a one-way ANOVA with post hoc Dunnett's multiple comparison test. Otherwise, analysis was instead performed by Mann-Whitney rank-sum test or Kruskal-Wallis test with Dunn's multiple comparison post hoc test. Statistical significance is indicated by *$p < 0.05$, **$p < 0.01$, and ***$p < 0.001$.

SUPPLEMENTAL INFORMATION

Supplemental Information includes Supplemental Materials and Methods, seven figures, and one table and can be found with this article online at https://doi.org/10.1016/j.ymthe.2018.10.010.

AUTHOR CONTRIBUTIONS

Conceptualization, H.W., C.E.H., and S.T.; Methodology, H.W., C.E.H., S.T., E.R.L., M.-H.L., K.J.S., H.L., D.J.W., P.H., L.A.W., J.S., K.C.K., and E.J.; Validation, H.W., S.T., and E.R.L.; Formal Analysis, H.W., S.T., E.R.L., M.-H.L., K.J.S., D.J.W., and L.A.W.; Investigation, H.W., S.T., E.R.L., M.-H.L., K.J.S., D.J.W., and L.A.W.; Resources, I.L., K.C.K., P.H., L.A.W., J.S., and K.E.; Writing – Original Draft, H.W., S.T., and E.R.L.; Writing – Review and Editing, H.W., S.T., E.R.L., C.E.H., and B.R.S.; Visualization, S.T., K.J.S., D.J.W., and L.A.W.; Supervision, H.W., C.E.H., and B.R.S.; Funding Acquisition, H.W., C.E.H., B.R.S., and K.E.

CONFLICTS OF INTEREST

H.W., C.E.H., and S.T. have filed an application for a patent regarding the use of TUDCA and related compounds in the prospective treatment of neurodegenerative disease (CU13092-0379639-TB.JK).

ACKNOWLEDGMENTS

We would like to thank Dr. Julia Kaltschmidt, for kindly providing transgenic mice used for the derivation of Ptf1α embryonic stem cell lines, and Caroline Lindblad and Arvid Frostell, for assistance with statistical analysis. This work was funded by Project ALS, Target ALS, the NIH (NS078097), and DoD (W81XWH-16-1-0204). S.T. received additional funding from the Swedish Wenner-Gren Foundation and The Foundation BLANCEFLOR Boncompagni Ludovisi, née Bildt.

REFERENCES

1. Peters, O.M., Ghasemi, M., and Brown, R.H., Jr. (2015). Emerging mechanisms of molecular pathology in ALS. J. Clin. Invest. *125*, 2548.
2. Chia, R., Chiò, A., and Traynor, B.J. (2018). Novel genes associated with amyotrophic lateral sclerosis: diagnostic and clinical implications. Lancet Neurol. *17*, 94–102.
3. Ilieva, H., Polymenidou, M., and Cleveland, D.W. (2009). Non-cell autonomous toxicity in neurodegenerative disorders: ALS and beyond. J. Cell Biol. *187*, 761–772.
4. Boillée, S., Yamanaka, K., Lobsiger, C.S., Copeland, N.G., Jenkins, N.A., Kassiotis, G., Kollias, G., and Cleveland, D.W. (2006). Onset and progression in inherited ALS determined by motor neurons and microglia. Science *312*, 1389–1392.
5. Di Giorgio, F.P., Boulting, G.L., Bobrowicz, S., and Eggan, K.C. (2008). Human embryonic stem cell-derived motor neurons are sensitive to the toxic effect of glial cells carrying an ALS-causing mutation. Cell Stem Cell *3*, 637–648.
6. Di Giorgio, F.P., Carrasco, M.A., Siao, M.C., Maniatis, T., and Eggan, K. (2007). Non-cell autonomous effect of glia on motor neurons in an embryonic stem cell-based ALS model. Nat. Neurosci. *10*, 608–614.
7. Kang, S.H., Li, Y., Fukaya, M., Lorenzini, I., Cleveland, D.W., Ostrow, L.W., Rothstein, J.D., and Bergles, D.E. (2013). Degeneration and impaired regeneration of gray matter oligodendrocytes in amyotrophic lateral sclerosis. Nat. Neurosci. *16*, 571–579.
8. Nagai, M., Re, D.B., Nagata, T., Chalazonitis, A., Jessell, T.M., Wichterle, H., and Przedborski, S. (2007). Astrocytes expressing ALS-linked mutated SOD1 release factors selectively toxic to motor neurons. Nat. Neurosci. *10*, 615–622.
9. Amoroso, M.W., Croft, G.F., Williams, D.J., O'Keeffe, S., Carrasco, M.A., Davis, A.R., Roybon, L., Oakley, D.H., Maniatis, T., Henderson, C.E., and Wichterle, H. (2013). Accelerated high-yield generation of limb-innervating motor neurons from human stem cells. J. Neurosci. *33*, 574–586.
10. Dimos, J.T., Rodolfa, K.T., Niakan, K.K., Weisenthal, L.M., Mitsumoto, H., Chung, W., Croft, G.F., Saphier, G., Leibel, R., Goland, R., et al. (2008). Induced pluripotent stem cells generated from patients with ALS can be differentiated into motor neurons. Science *321*, 1218–1221.
11. Höing, S., Rudhard, Y., Reinhardt, P., Glatza, M., Stehling, M., Wu, G., Peiker, C., Böcker, A., Parga, J.A., Bunk, E., et al. (2012). Discovery of inhibitors of microglial neurotoxicity acting through multiple mechanisms using a stem-cell-based phenotypic assay. Cell Stem Cell *11*, 620–632.
12. Wichterle, H., Lieberam, I., Porter, J.A., and Jessell, T.M. (2002). Directed differentiation of embryonic stem cells into motor neurons. Cell *110*, 385–397.
13. Yang, Y.M., Gupta, S.K., Kim, K.J., Powers, B.E., Cerqueira, A., Wainger, B.J., Ngo, H.D., Rosowski, K.A., Schein, P.A., Ackeifi, C.A., et al. (2013). A small molecule screen in stem-cell-derived motor neurons identifies a kinase inhibitor as a candidate therapeutic for ALS. Cell Stem Cell *12*, 713–726.
14. Patterson, M., Chan, D.N., Ha, I., Case, D., Cui, Y., Van Handel, B., Mikkola, H.K., and Lowry, W.E. (2012). Defining the nature of human pluripotent stem cell progeny. Cell Res. *22*, 178–193.
15. Stein, J.L., de la Torre-Ubieta, L., Tian, Y., Parikshak, N.N., Hernández, I.A., Marchetto, M.C., Baker, D.K., Lu, D., Hinman, C.R., Lowe, J.K., et al. (2014). A quantitative framework to evaluate modeling of cortical development by neural stem cells. Neuron *83*, 69–86.
16. Miles, G.B., Yohn, D.C., Wichterle, H., Jessell, T.M., Rafuse, V.F., and Brownstone, R.M. (2004). Functional properties of motoneurons derived from mouse embryonic stem cells. J. Neurosci. *24*, 7848–7858.
17. Jacko, M., Weyn-Vanhentenryck, S.M., Smerdon, J.W., Yan, R., Feng, H., Williams, D.J., Pai, J., Xu, K., Wichterle, H., and Zhang, C. (2018). Rbfox Splicing Factors Promote Neuronal Maturation and Axon Initial Segment Assembly. Neuron *97*, 853–868.e6.
18. Bosco, D.A., Morfini, G., Karabacak, N.M., Song, Y., Gros-Louis, F., Pasinelli, P., Goolsby, H., Fontaine, B.A., Lemay, N., McKenna-Yasek, D., et al. (2010). Wild-type and mutant SOD1 share an aberrant conformation and a common pathogenic pathway in ALS. Nat. Neurosci. *13*, 1396–1403.
19. Kiskinis, E., Sandoe, J., Williams, L.A., Boulting, G.L., Moccia, R., Wainger, B.J., Han, S., Peng, T., Thams, S., Mikkilineni, S., et al. (2014). Pathways disrupted in human ALS motor neurons identified through genetic correction of mutant SOD1. Cell Stem Cell *14*, 781–795.
20. Wang, J., Farr, G.W., Zeiss, C.J., Rodriguez-Gil, D.J., Wilson, J.H., Furtak, K., Rutkowski, D.T., Kaufman, R.J., Ruse, C.I., Yates, J.R., 3rd, et al. (2009). Progressive aggregation despite chaperone associations of a mutant SOD1-YFP in transgenic mice that develop ALS. Proc. Natl. Acad. Sci. USA *106*, 1392–1397.
21. Alami, N.H., Smith, R.B., Carrasco, M.A., Williams, L.A., Winborn, C.S., Han, S.S.W., Kiskinis, E., Winborn, B., Freibaum, B.D., Kanagaraj, A., et al. (2014). Axonal transport of TDP-43 mRNA granules is impaired by ALS-causing mutations. Neuron *81*, 536–543.
22. Devlin, A.C., Burr, K., Borooah, S., Foster, J.D., Cleary, E.M., Geti, I., Vallier, L., Shaw, C.E., Chandran, S., and Miles, G.B. (2015). Human iPSC-derived motoneurons harbouring TARDBP or C9ORF72 ALS mutations are dysfunctional despite maintaining viability. Nat. Commun. *6*, 5999.
23. Donnelly, C.J., Zhang, P.W., Pham, J.T., Haeusler, A.R., Mistry, N.A., Vidensky, S., Daley, E.L., Poth, E.M., Hoover, B., Fines, D.M., et al. (2013). RNA toxicity from the ALS/FTD C9ORF72 expansion is mitigated by antisense intervention. Neuron *80*, 415–428.
24. Egawa, N., Kitaoka, S., Tsukita, K., Naitoh, M., Takahashi, K., Yamamoto, T., Adachi, F., Kondo, T., Okita, K., Asaka, I., et al. (2012). Drug screening for ALS using patient-specific induced pluripotent stem cells. Sci. Transl. Med. *4*, 145ra104.
25. Naujock, M., Stanslowsky, N., Bufler, S., Naumann, M., Reinhardt, P., Sterneckert, J., Kefalakes, E., Kassebaum, C., Bursch, F., Lojewski, X., et al. (2016). 4-Aminopyridine Induced Activity Rescues Hypoexcitable Motor Neurons from Amyotrophic Lateral Sclerosis Patient-Derived Induced Pluripotent Stem Cells. Stem Cells *34*, 1563–1575.
26. Sareen, D., O'Rourke, J.G., Meera, P., Muhammad, A.K., Grant, S., Simpkinson, M., Bell, S., Carmona, S., Ornelas, L., Sahabian, A., et al. (2013). Targeting RNA foci in iPSC-derived motor neurons from ALS patients with a C9ORF72 repeat expansion. Sci. Transl. Med. *5*, 208ra149.
27. Sivadasan, R., Hornburg, D., Drepper, C., Frank, N., Jablonka, S., Hansel, A., Lojewski, X., Sterneckert, J., Hermann, A., Shaw, P.J., et al. (2016). C9ORF72 interaction with cofilin modulates actin dynamics in motor neurons. Nat. Neurosci. *19*, 1610–1618.
28. Wainger, B.J., Kiskinis, E., Mellin, C., Wiskow, O., Han, S.S., Sandoe, J., Perez, N.P., Williams, L.A., Lee, S., Boulting, G., et al. (2014). Intrinsic membrane hyperexcitability of amyotrophic lateral sclerosis patient-derived motor neurons. Cell Rep. *7*, 1–11.
29. Gurney, M.E., Pu, H., Chiu, A.Y., Dal Canto, M.C., Polchow, C.Y., Alexander, D.D., Caliendo, J., Hentati, A., Kwon, Y.W., Deng, H.X., et al. (1994). Motor neuron degeneration in mice that express a human Cu,Zn superoxide dismutase mutation. Science *264*, 1772–1775.
30. Goeger, D.E., Riley, R.T., Dorner, J.W., and Cole, R.J. (1988). Cyclopiazonic acid inhibition of the Ca2+-transport ATPase in rat skeletal muscle sarcoplasmic reticulum vesicles. Biochem. Pharmacol. *37*, 978–981.
31. Doutheil, J., Gissel, C., Oschlies, U., Hossmann, K.A., and Paschen, W. (1997). Relation of neuronal endoplasmic reticulum calcium homeostasis to ribosomal aggregation and protein synthesis: implications for stress-induced suppression of protein synthesis. Brain Res. *775*, 43–51.
32. Hetz, C., and Saxena, S. (2017). ER stress and the unfolded protein response in neurodegeneration. Nat. Rev. Neurol. *13*, 477–491.
33. Hetz, C., Thielen, P., Matus, S., Nassif, M., Court, F., Kiffin, R., Martinez, G., Cuervo, A.M., Brown, R.H., and Glimcher, L.H. (2009). XBP-1 deficiency in the nervous system protects against amyotrophic lateral sclerosis by increasing autophagy. Genes Dev. *23*, 2294–2306.
34. Saxena, S., Cabuy, E., and Caroni, P. (2009). A role for motoneuron subtype-selective ER stress in disease manifestations of FALS mice. Nat. Neurosci. *12*, 627–636.
35. Saxena, S., Roselli, F., Singh, K., Leptien, K., Julien, J.P., Gros-Louis, F., and Caroni, P. (2013). Neuroprotection through excitability and mTOR required in ALS motoneurons to delay disease and extend survival. Neuron *80*, 80–96.
36. Kramer, N.J., Haney, M.S., Morgens, D.W., Jovičić, A., Couthouis, J., Li, A., Ousey, J., Ma, R., Bieri, G., Tsui, C.K., et al. (2018). CRISPR-Cas9 screens in human cells and primary neurons identify modifiers of C9ORF72 dipeptide-repeat-protein toxicity. Nat. Genet. *50*, 603–612.

37. Atkin, J.D., Farg, M.A., Walker, A.K., McLean, C., Tomas, D., and Horne, M.K. (2008). Endoplasmic reticulum stress and induction of the unfolded protein response in human sporadic amyotrophic lateral sclerosis. Neurobiol. Dis. *30*, 400–407.

38. Kanning, K.C., Kaplan, A., and Henderson, C.E. (2010). Motor neuron diversity in development and disease. Annu. Rev. Neurosci. *33*, 409–440.

39. Nijssen, J., Comley, L.H., and Hedlund, E. (2017). Motor neuron vulnerability and resistance in amyotrophic lateral sclerosis. Acta Neuropathol. *133*, 863–885.

40. Kaplan, A., Spiller, K.J., Towne, C., Kanning, K.C., Choe, G.T., Geber, A., Akay, T., Aebischer, P., and Henderson, C.E. (2014). Neuronal matrix metalloproteinase-9 is a determinant of selective neurodegeneration. Neuron *81*, 333–348.

41. Liu, M.L., Zang, T., and Zhang, C.L. (2016). Direct Lineage Reprogramming Reveals Disease-Specific Phenotypes of Motor Neurons from Human ALS Patients. Cell Rep. *14*, 115–128.

42. Hanson, M.G., Jr., Shen, S., Wiemelt, A.P., McMorris, F.A., and Barres, B.A. (1998). Cyclic AMP elevation is sufficient to promote the survival of spinal motor neurons in vitro. J. Neurosci. *18*, 7361–7371.

43. Haidet-Phillips, A.M., Hester, M.E., Miranda, C.J., Meyer, K., Braun, L., Frakes, A., Song, S., Likhite, S., Murtha, M.J., Foust, K.D., et al. (2011). Astrocytes from familial and sporadic ALS patients are toxic to motor neurons. Nat. Biotechnol. *29*, 824–828.

44. Rowland, L.P., and Shneider, N.A. (2001). Amyotrophic lateral sclerosis. N. Engl. J. Med. *344*, 1688–1700.

45. Hoang, P.T., Chalif, J.I., Bikoff, J.B., Jessell, T.M., Mentis, G.Z., and Wichterle, H. (2018). Subtype Diversification and Synaptic Specificity of Stem Cell-Derived Spinal Interneurons. Neuron *100*, 135–149.e7.

46. De Stefani, D., Bononi, A., Romagnoli, A., Messina, A., De Pinto, V., Pinton, P., and Rizzuto, R. (2012). VDAC1 selectively transfers apoptotic Ca2+ signals to mitochondria. Cell Death Differ. *19*, 267–273.

47. Jayaraman, T., and Marks, A.R. (1997). T cells deficient in inositol 1,4,5-trisphosphate receptor are resistant to apoptosis. Mol. Cell. Biol. *17*, 3005–3012.

48. Pinton, P., Giorgi, C., Siviero, R., Zecchini, E., and Rizzuto, R. (2008). Calcium and apoptosis: ER-mitochondria Ca2+ transfer in the control of apoptosis. Oncogene *27*, 6407–6418.

49. Bernard-Marissal, N., Moumen, A., Sunyach, C., Pellegrino, C., Dudley, K., Henderson, C.E., Raoul, C., and Pettmann, B. (2012). Reduced calreticulin levels link endoplasmic reticulum stress and Fas-triggered cell death in motoneurons vulnerable to ALS. J. Neurosci. *32*, 4901–4912.

50. Jaiswal, M.K., and Keller, B.U. (2009). Cu/Zn superoxide dismutase typical for familial amyotrophic lateral sclerosis increases the vulnerability of mitochondria and perturbs Ca2+ homeostasis in SOD1G93A mice. Mol. Pharmacol. *75*, 478–489.

51. Jaiswal, M.K., Zech, W.D., Goos, M., Leutbecher, C., Ferri, A., Zippelius, A., Carrì, M.T., Nau, R., and Keller, B.U. (2009). Impairment of mitochondrial calcium handling in a mtSOD1 cell culture model of motoneuron disease. BMC Neurosci. *10*, 64.

52. Kawamata, H., and Manfredi, G. (2010). Mitochondrial dysfunction and intracellular calcium dysregulation in ALS. Mech. Ageing Dev. *131*, 517–526.

53. Kim, H.J., Magranè, J., Starkov, A.A., and Manfredi, G. (2012). The mitochondrial calcium regulator cyclophilin D is an essential component of oestrogen-mediated neuroprotection in amyotrophic lateral sclerosis. Brain *135*, 2865–2874.

54. Rothstein, J.D., Tsai, G., Kuncl, R.W., Clawson, L., Cornblath, D.R., Drachman, D.B., Pestronk, A., Stauch, B.L., and Coyle, J.T. (1990). Abnormal excitatory amino acid metabolism in amyotrophic lateral sclerosis. Ann. Neurol. *28*, 18–25.

55. Takuma, H., Kwak, S., Yoshizawa, T., and Kanazawa, I. (1999). Reduction of GluR2 RNA editing, a molecular change that increases calcium influx through AMPA receptors, selective in the spinal ventral gray of patients with amyotrophic lateral sclerosis. Ann. Neurol. *46*, 806–815.

56. Tradewell, M.L., Cooper, L.A., Minotti, S., and Durham, H.D. (2011). Calcium dysregulation, mitochondrial pathology and protein aggregation in a culture model of amyotrophic lateral sclerosis: mechanistic relationship and differential sensitivity to intervention. Neurobiol. Dis. *42*, 265–275.

57. von Lewinski, F., and Keller, B.U. (2005). Ca2+, mitochondria and selective motoneuron vulnerability: implications for ALS. Trends Neurosci. *28*, 494–500.

58. Pirot, P., Eizirik, D.L., and Cardozo, A.K. (2006). Interferon-gamma potentiates endoplasmic reticulum stress-induced death by reducing pancreatic beta cell defence mechanisms. Diabetologia *49*, 1229–1236.

59. Gardner, B.M., Pincus, D., Gotthardt, K., Gallagher, C.M., and Walter, P. (2013). Endoplasmic reticulum stress sensing in the unfolded protein response. Cold Spring Harb. Perspect. Biol. *5*, a013169.

60. Hetz, C. (2012). The unfolded protein response: controlling cell fate decisions under ER stress and beyond. Nat. Rev. Mol. Cell Biol. *13*, 89–102.

61. Iurlaro, R., and Muñoz-Pinedo, C. (2016). Cell death induced by endoplasmic reticulum stress. FEBS J. *283*, 2640–2652.

62. Kozutsumi, Y., Segal, M., Normington, K., Gething, M.J., and Sambrook, J. (1988). The presence of malfolded proteins in the endoplasmic reticulum signals the induction of glucose-regulated proteins. Nature *332*, 462–464.

63. Urano, F., Wang, X., Bertolotti, A., Zhang, Y., Chung, P., Harding, H.P., and Ron, D. (2000). Coupling of stress in the ER to activation of JNK protein kinases by transmembrane protein kinase IRE1. Science *287*, 664–666.

64. Sun, S., Sun, Y., Ling, S.C., Ferraiuolo, L., McAlonis-Downes, M., Zou, Y., Drenner, K., Wang, Y., Ditsworth, D., Tokunaga, S., et al. (2015). Translational profiling identifies a cascade of damage initiated in motor neurons and spreading to glia in mutant SOD1-mediated ALS. Proc. Natl. Acad. Sci. USA *112*, E6993–E7002.

65. Gros-Louis, F., Soucy, G., Larivière, R., and Julien, J.P. (2010). Intracerebroventricular infusion of monoclonal antibody or its derived Fab fragment against misfolded forms of SOD1 mutant delays mortality in a mouse model of ALS. J. Neurochem. *113*, 1188–1199.

66. Nishitoh, H., Kadowaki, H., Nagai, A., Maruyama, T., Yokota, T., Fukutomi, H., Noguchi, T., Matsuzawa, A., Takeda, K., and Ichijo, H. (2008). ALS-linked mutant SOD1 induces ER stress- and ASK1-dependent motor neuron death by targeting Derlin-1. Genes Dev. *22*, 1451–1464.

67. Sakaki, K., Wu, J., and Kaufman, R.J. (2008). Protein kinase Ctheta is required for autophagy in response to stress in the endoplasmic reticulum. J. Biol. Chem. *283*, 15370–15380.

68. Kase, H., Iwahashi, K., Nakanishi, S., Matsuda, Y., Yamada, K., Takahashi, M., Murakata, C., Sato, A., and Kaneko, M. (1987). K-252 compounds, novel and potent inhibitors of protein kinase C and cyclic nucleotide-dependent protein kinases. Biochem. Biophys. Res. Commun. *142*, 436–440.

69. Roux, P.P., Dorval, G., Boudreau, M., Angers-Loustau, A., Morris, S.J., Makkerh, J., and Barker, P.A. (2002). K252a and CEP1347 are neuroprotective compounds that inhibit mixed-lineage kinase-3 and induce activation of Akt and ERK. J. Biol. Chem. *277*, 49473–49480.

70. Maury, Y., Côme, J., Piskorowski, R.A., Salah-Mohellibi, N., Chevaleyre, V., Peschanski, M., Martinat, C., and Nedelec, S. (2015). Combinatorial analysis of developmental cues efficiently converts human pluripotent stem cells into multiple neuronal subtypes. Nat. Biotechnol. *33*, 89–96.

71. Elia, A.E., Lalli, S., Monsurrò, M.R., Sagnelli, A., Taiello, A.C., Reggiori, B., La Bella, V., Tedeschi, G., and Albanese, A. (2016). Tauroursodeoxycholic acid in the treatment of patients with amyotrophic lateral sclerosis. Eur. J. Neurol. *23*, 45–52.

72. Kaemmerer, W.F., Rodrigues, C.M., Steer, C.J., and Low, W.C. (2001). Creatine-supplemented diet extends Purkinje cell survival in spinocerebellar ataxia type 1 transgenic mice but does not prevent the ataxic phenotype. Neuroscience *103*, 713–724.

73. Azzouz, M., Leclerc, N., Gurney, M., Warter, J.M., Poindron, P., and Borg, J. (1997). Progressive motor neuron impairment in an animal model of familial amyotrophic lateral sclerosis. Muscle Nerve *20*, 45–51.

74. Maselli, R.A., Wollman, R.L., Leung, C., Distad, B., Palombi, S., Richman, D.P., Salazar-Grueso, E.F., and Roos, R.P. (1993). Neuromuscular transmission in amyotrophic lateral sclerosis. Muscle Nerve *16*, 1193–1203.

75. Tsujihata, M., Hazama, R., Yoshimura, T., Satoh, A., Mori, M., and Nagataki, S. (1984). The motor end-plate fine structure and ultrastructural localization of acetylcholine receptors in amyotrophic lateral sclerosis. Muscle Nerve *7*, 243–249.

76. Sharma, A., Lyashchenko, A.K., Lu, L., Nasrabady, S.E., Elmaleh, M., Mendelsohn, M., Nemes, A., Tapia, J.C., Mentis, G.Z., and Shneider, N.A. (2016). ALS-associated mutant FUS induces selective motor neuron degeneration through toxic gain of function. Nat. Commun. *7*, 10465.

77. Chiu, A.Y., Zhai, P., Dal Canto, M.C., Peters, T.M., Kwon, Y.W., Prattis, S.M., and Gurney, M.E. (1995). Age-dependent penetrance of disease in a transgenic mouse model of familial amyotrophic lateral sclerosis. Mol. Cell. Neurosci. *6*, 349–362.

78. Cai, Y., Arikkath, J., Yang, L., Guo, M.L., Periyasamy, P., and Buch, S. (2016). Interplay of endoplasmic reticulum stress and autophagy in neurodegenerative disorders. Autophagy *12*, 225–244.

79. Meares, G.P., Mines, M.A., Beurel, E., Eom, T.Y., Song, L., Zmijewska, A.A., and Jope, R.S. (2011). Glycogen synthase kinase-3 regulates endoplasmic reticulum (ER) stress-induced CHOP expression in neuronal cells. Exp. Cell Res. *317*, 1621–1628.

80. Jeohn, G.H., Wilson, B., Wetsel, W.C., and Hong, J.S. (2000). The indolocarbazole Gö6976 protects neurons from lipopolysaccharide/interferon-gamma-induced cytotoxicity in murine neuron/glia co-cultures. Brain Res. Mol. Brain Res. *79*, 32–44.

81. Pakos-Zebrucka, K., Koryga, I., Mnich, K., Ljujic, M., Samali, A., and Gorman, A.M. (2016). The integrated stress response. EMBO Rep. *17*, 1374–1395.

82. Wek, R.C. (2018). Role of eIF2α Kinases in Translational Control and Adaptation to Cellular Stress. Cold Spring Harb. Perspect. Biol. *10*, a032870.

83. Leost, M., Schultz, C., Link, A., Wu, Y.Z., Biernat, J., Mandelkow, E.M., Bibb, J.A., Snyder, G.L., Greengard, P., Zaharevitz, D.W., et al. (2000). Paullones are potent inhibitors of glycogen synthase kinase-3beta and cyclin-dependent kinase 5/p25. Eur. J. Biochem. *267*, 5983–5994.

84. Schultz, C., Link, A., Leost, M., Zaharevitz, D.W., Gussio, R., Sausville, E.A., Meijer, L., and Kunick, C. (1999). Paullones, a series of cyclin-dependent kinase inhibitors: synthesis, evaluation of CDK1/cyclin B inhibition, and in vitro antitumor activity. J. Med. Chem. *42*, 2909–2919.

85. Lemonnier, J., Ghayor, C., Guicheux, J., and Caverzasio, J. (2004). Protein kinase C-independent activation of protein kinase D is involved in BMP-2-induced activation of stress mitogen-activated protein kinases JNK and p38 and osteoblastic cell differentiation. J. Biol. Chem. *279*, 259–264.

86. Sun, K.H., Lee, H.G., Smith, M.A., and Shah, K. (2009). Direct and indirect roles of cyclin-dependent kinase 5 as an upstream regulator in the c-Jun NH2-terminal kinase cascade: relevance to neurotoxic insults in Alzheimer's disease. Mol. Biol. Cell *20*, 4611–4619.

87. Keene, C.D., Rodrigues, C.M., Eich, T., Chhabra, M.S., Steer, C.J., and Low, W.C. (2002). Tauroursodeoxycholic acid, a bile acid, is neuroprotective in a transgenic animal model of Huntington's disease. Proc. Natl. Acad. Sci. USA *99*, 10671–10676.

88. Keene, C.D., Rodrigues, C.M., Eich, T., Linehan-Stieers, C., Abt, A., Kren, B.T., Steer, C.J., and Low, W.C. (2001). A bile acid protects against motor and cognitive deficits and reduces striatal degeneration in the 3-nitropropionic acid model of Huntington's disease. Exp. Neurol. *171*, 351–360.

89. Nunes, A.F., Amaral, J.D., Lo, A.C., Fonseca, M.B., Viana, R.J., Callaerts-Vegh, Z., D'Hooge, R., and Rodrigues, C.M. (2012). TUDCA, a bile acid, attenuates amyloid precursor protein processing and amyloid-β deposition in APP/PS1 mice. Mol. Neurobiol. *45*, 440–454.

90. Ackerman, H.D., and Gerhard, G.S. (2016). Bile Acids in Neurodegenerative Disorders. Front. Aging Neurosci. *8*, 263.

91. Castro-Caldas, M., Carvalho, A.N., Rodrigues, E., Henderson, C.J., Wolf, C.R., Rodrigues, C.M., and Gama, M.J. (2012). Tauroursodeoxycholic acid prevents MPTP-induced dopaminergic cell death in a mouse model of Parkinson's disease. Mol. Neurobiol. *46*, 475–486.

92. Ozcan, U., Yilmaz, E., Ozcan, L., Furuhashi, M., Vaillancourt, E., Smith, R.O., Görgün, C.Z., and Hotamisligil, G.S. (2006). Chemical chaperones reduce ER stress and restore glucose homeostasis in a mouse model of type 2 diabetes. Science *313*, 1137–1140.

93. Uppala, J.K., Gani, A.R., and Ramaiah, K.V.A. (2017). Chemical chaperone, TUDCA unlike PBA, mitigates protein aggregation efficiently and resists ER and non-ER stress induced HepG2 cell death. Sci. Rep. *7*, 3831.

94. Kawaguchi, Y., Cooper, B., Gannon, M., Ray, M., MacDonald, R.J., and Wright, C.V. (2002). The role of the transcriptional regulator Ptf1a in converting intestinal to pancreatic progenitors. Nat. Genet. *32*, 128–134.

95. Madisen, L., Zwingman, T.A., Sunkin, S.M., Oh, S.W., Zariwala, H.A., Gu, H., Ng, L.L., Palmiter, R.D., Hawrylycz, M.J., Jones, A.R., et al. (2010). A robust and high-throughput Cre reporting and characterization system for the whole mouse brain. Nat. Neurosci. *13*, 133–140.

96. Maeder, M.L., Thibodeau-Beganny, S., Osiak, A., Wright, D.A., Anthony, R.M., Eichtinger, M., Jiang, T., Foley, J.E., Winfrey, R.J., Townsend, J.A., et al. (2008). Rapid "open-source" engineering of customized zinc-finger nucleases for highly efficient gene modification. Mol. Cell *31*, 294–301.

97. Johnson-Kerner, B.L., Ahmad, F.S., Diaz, A.G., Greene, J.P., Gray, S.J., Samulski, R.J., Chung, W.K., Van Coster, R., Maertens, P., Noggle, S.A., et al. (2015). Intermediate filament protein accumulation in motor neurons derived from giant axonal neuropathy iPSCs rescued by restoration of gigaxonin. Hum. Mol. Genet. *24*, 1420–1431.

YMTHE, Volume *27*

Supplemental Information

A Stem Cell-Based Screening Platform Identifies Compounds that Desensitize Motor Neurons to Endoplasmic Reticulum Stress

Sebastian Thams, Emily Rhodes Lowry, Marie-Hélène Larraufie, Krista J. Spiller, Hai Li, Damian J. Williams, Phuong Hoang, Elise Jiang, Luis A. Williams, Jackson Sandoe, Kevin Eggan, Ivo Lieberam, Kevin C. Kanning, Brent R. Stockwell, Christopher E. Henderson, and Hynek Wichterle

Supplemental materials and methods

Automated image analysis

To assess the number of "healthy" fluorescent cells exhibiting outgrowths >5 times the cell body diameter (assessment of overall survival) and to evaluate the mean neurite length per cell (assessment of neurite growth). These parameters were used consistently throughout the study.

Small molecule screen

We consistently observed that the ratio of surviving untreated G93A mutant motor neurons to untreated wild-type motor neurons was ~0.83; in order to detect compounds acting synergistically to the genotype, all data were normalized to this ratio. Compounds resulting in a G93A-to-WT survival ratio of <0.67-fold, corresponding to a 50% difference in survival, were re-tested in five-point 2-fold dilution series. All hit compounds were evaluated visually, and wells with apparent artefacts such as auto-fluorescence and excessive cell clumping were removed. Compounds that were generally toxic, i.e., that resulted in lower survival than the controls with low trophic support for both genotypes, were rescreened in 1:10 dilution series. After completion of screen data collection, images for all hit compounds were individually evaluated in blinded manner. Wells with overall low survival or artefacts (e.g. precipitation, auto-fluorescence or significant cell detachment, were excluded for further analysis). The remaining compounds were tested in 8-point dose response titrations, in FACS-purified cultures and in an independent pair of mutant-wild type cell lines.

Immunohistochemistry

Cultures were washed three times with 0.01 M PBS containing 0.3% Triton-X, prior to incubation with secondary antibodies (Alexa donkey 488/555/647) for 60 min in room temperature. The following primary antibodies were used: mouse Hb9 and mouse islet1/2 from Hybridoma Bank (1:100); mouse Human nuclear antigen from Millipore (MAB1281, clone 235-1, 1:1000); Tuj-1 from Neuromics or EMD Millipore (1:500); and phospho c-jun from Cell Signalling (1:100). Slides were examined in either a Zeiss AxioObserver with a Coolsnap HQ_2 camera (Photometrics), a Zeiss LSM Meta 510 or a Zeiss LSM 880 Axioobserver Z1 confocal microscope. Images were processed and sometimes cropped in Adobe Photoshop (Creative suit 6, Adobe Systems) for presentations purpose, changes were applied to the entire image, and in equal proportions to all images from the same.

Calcium imaging

On day three post-dissociation, coverslips were incubated with 5 μM Fura-2 AM, ratiometric calcium indicator dye (Life Sciences, USA) for 30 minutes at room temperature. After washing, coverslips were mounted on a Nikon Eclipse TE 3500 inverted microscope equipped with a 40× 1.30 NA objective (Nikon, USA), a pco.EDGE CMOS camera (pco, Germany), a Lambda LS light source, a Lambda LS-2 filterwheel with 340 nm and 380 nm excitation filters (both Sutter, USA). Images were first acquired using bright field and a fluorescent filter to identify cells to analyze at later steps. Drug applications were carried out using a custom-built focal application system located approximately 100 μm from the field of view. A 5 s baseline for the Fura-2 signal was then acquired, followed by a 1 s pulse of 100 μM kainic acid (KA). Epifluorescent images were captured at a rate of 1 image/sec for 1 min, switching between 340 and 380 nm filters every 500 ms. Cells were allowed to recover for 2 min, and only coverslips where cells returned to baseline were analyzed further. The coverslips were then continuously exposed to 7.5 μM CPA while 1 image/30 sec was acquired for 20 min, followed by a 2 min recovery, and finally a second pulse of KA. Following acquisition, the 340/380 ratio of each pair of images was calculated on a pixel by pixel basis using FIJI software v. 1.4 (www.fiji.sc). Regions of interest were drawn manually using the morphology of the cells from a single 340 image as a template. Quantification was carried out using Igor Pro v. 6 (Wavemetrics, USA). The rate at which the evoked calcium transients returned to the baseline was calculated from the tau (time constant) of a single exponential curve fitted to the falling part of the Ca intensity trace from 80% to 20% of the peak. Only neurons that recovered to 10% of the peak ratio value were included in the analysis.

qPCR primers

Xbp1_1_fwd	ACA CGC TTG GGA ATG GAC AC
Xbp1_1_rev	CCA TGG GAA GAT GTT CTG GG
Xbp1_2_fwd	GAA TGC CCA AAA GGA TAT CAG ACT C
Xbp1_2_rev	GGC CTT GTG GTT GAG AAC CAG GAG
p58ipk_fwd	TGG ACT TTA CTG CCG CAA GA
p58ipk_rev	CGT CAA GCT TCC CTT GTT TGA
Gapdh_fwd	CAT GGC CTT CCG TGT TCC TA
Gapdh_rev	GCG GCA CGT CAG ATC CA
Erdj4_fwd	CCT TTC ACA AAT TAG CCA TGA AGT AC
Erdj4_rev	TGC TTC AGC ATC AGG GCT TT
Chop_fwd	AGG AGC CAG GGC CAA CA
Chop_rev	TCT GGA GAG CGA GGG CTT T
Cd59a_fwd	GCT GCT TCT GGC TGT GTT CTG
Cd59a_rev	GTT GGA AAC AGT GGT AGC ATG TG
Bloc1s1_fwd	CAG GCC TAC ATG AAC CAG AGA AA
Bloc1s1_rev	GGC AGC CTG GAC CTG TAG AG
Nfkb2_fwd	GTG GGC AAG CAG TGT TCA GA
Nfkb2_rev	TCA TGT CCT TGG GTC CTA CAG A
Tnfrsf10b_fwd	CGT CTC ATG CGG CAG TTG
Tnfrsf10b_rev	TCG GCT TTG ACC ATT TGG A
Creb3l3_fwd	CCA GCT GCC TCT CAC CAA GT
Creb3l3_rev	CCG GAT CTT TCT GCG GAT T
Noxa_fwd	CTG TGG TTC TGG CGC AGA T
Noxa_rev	GGG CTT GGG CTC CTC ATC
Nrf2_fwd	TTC CCG TGA GTC CTG GTC AT
Nrf2_rev	AGC GGC TTG AAT GTT TGT CTT T
Tap1_fwd	TTG GCC CGA GCC TTG A
Tap1_rev	TGG TGG CAT CAT CCA AGA TAA G
Bip_fwd	AGC CAT CCC GTG GCA TAA
Bip_rev	GGA CAG CGG CAC CAT AGG
Calr_fwd	GCC AGA CAC TGG TGG TAC AGT TC
Calr_rev	CGC CCC CAC AGT CGA TAT T
Gadd45a_fwd	GAC GAC GAC CGG GAT GTG
Gadd45a_rev	AGC AGA ACG CAC GGA TGA G
Atf4_fwd	CGA TGC TCT GTT TCG AAT GGA
Atf4_rev	CCA ACG TGG TCA AGA GCT CAT

RNA-sequencing

RNA was isolated in duplicates from FACS-purified untreated, CPA treated and CPA + TUDCA treated MNS of both genotypes ($hSOD1^{WT}$ and $hSOD1^{G93A}$), as described for RT-qPCR reactions. Poly-A pull-down was then used to enrich mRNAs from total RNA samples (1 µg per sample, RIN >8) and libraries were prepared using Illumina TruSeq RNA prep kit (San Diego, CA). Libraries were then sequenced using an Illumina HiSeq 2000 instrument (Columbia Genome Center, Columbia University). Read alignment and gene levels were calculated using Cufflinks and Tophat softwares. Raw FastQ sequencing data and processed normalized expression data (RPKM) were compared between. All genes associated with ER stress and associated pathways, suggested in the current literature, were selected for further analysis.

Generation isogenic human embryonic stem cell lines by genetic targeting

After corroborating the desired SOD1 gene edit (Fig. S5B-C), we directed the differentiation of SOD +/A4V and SOD1+/+ HUES3 Hb9::GFP cells into cultures containing spinal motor neurons. GFP^{+} motor neurons of both genotypes could be isolated using FACS (Fig. S5F), and SOD1 transcript and protein expression in these cells was confirmed (Fig. S5D-E). The new lines were further validated by staining for motor neuron transcription factor Islet1 (Fig. S5G) and assessment of survival in short and long term cultures (Figure S5H and J).

In vivo administration of TUDCA

Drug was administered every three days from P30 to P51 for a total of 7 injections. At P51, mice were deeply anesthetized using ketamine/xylazine and intracardially perfused with ~15 mL room temperature phosphate-buffered saline (PBS) followed by ~30 mL of 4% PFA. Following dissection, tibialis anterior (TA) muscles were washed in PBS overnight, and then processed for cryoprotective embedding. To visualize NMJs, 30 μm longitudinal cryosections of the whole TAs were incubated with α-bungarotoxin conjugated to Alexa Fluor 488 (1:500; Invitrogen) and an antibody to vesicular acetylcholine transporter (VAChT; raised in rabbit, Covance 1:32,000) to label motor endplates and nerve terminals, respectively. Because a lack of co-localization indicated muscle denervation, % NMJ innervation was determined by dividing the total number of areas of overlap between VAChT and BTX signals (total number innervated endplates) by the number of areas containing BTX signal (total number of endplates). One TA was assessed for each animal (n=4-6), with every third section throughout the whole muscle stained and counted such that a minimum of 1000 NMJs were evaluated per animal. Images were acquired using a Nikon Eclipse TE-2000-E fluorescence microscope with a 4x or 10x objective. All animal work was performed in compliance with Columbia University IACUC protocols.

Statistics

For cell cultures, a minimum of three independent experiments were generally performed, which was considered sufficient based on previous experience with this type of assays where culture conditions and cell lines were kept constant. For *in vivo* experiments, a power analysis based on pilot studies was performed to estimate the number of animals required to detect the studied effects. Data sets are expressed as mean value +/- SEM throughout the paper. Statistical analyses were performed with Graph Pad Prism (v. 7, GraphPad Software Inc.) or R' (www.r-project.org). If normal distribution and equal variance could be assumed, analysis of significance was performed with an unpaired two-tailed Student's t-test for pairwise comparison, or a One-way Anova with *post hoc* Dunnet's multiple comparison test. Otherwise, analysis was instead performed by Mann-Whitney Rank sum test or Kruskal-Wallis test with Dunn's multiple comparison *post hoc* test. Statistical significance is indicated by * $P<0.05$, ** $P<0.01$, *** $P<0.001$. Unless stated otherwise, each *N* represents an independent experiment or animal. In the few events where only one biological replicate was analyzed, the technical replicates were used to generate histograms, as stated in the figure legends when applicable. Statistical analyses were not performed on any of these data.

Figure S1

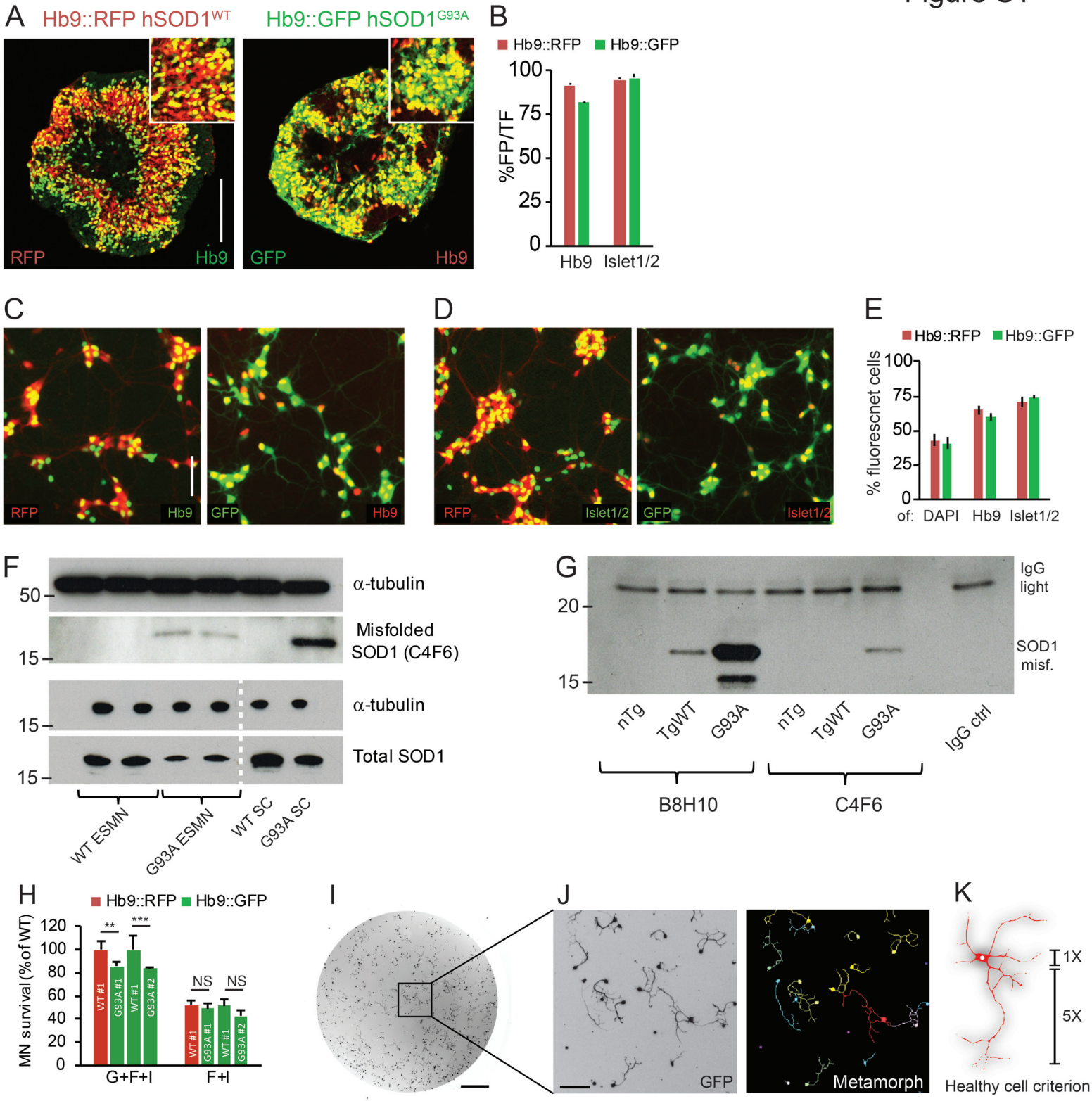
A
Hb9::RFP hSOD1WT
Hb9::GFP hSOD1G93A
RFP
Hb9
GFP
Hb9
B
Hb9::RFP
Hb9::GFP
%FP/TF
100
75
50
25
0
Hb9
Islet1/2
C
RFP
Hb9
GFP
Hb9
D
RFP
Islet1/2
GFP
Islet1/2
E
Hb9::RFP
Hb9::GFP
% fluorescnet cells
100
75
50
25
0
of:
DAPI
Hb9
Islet1/2
F
50
15
15
15
α-tubulin
Misfolded SOD1 (C4F6)
α-tubulin
Total SOD1
WT ESMN
G93A ESMN
WT SC
G93A SC
G
20
15
IgG light
SOD1 misf.
nTg
TgWT
G93A
nTg
TgWT
G93A
IgG ctrl
B8H10
C4F6
H
Hb9::RFP
Hb9::GFP
MN survival (% of WT)
120
100
80
60
40
20
0
**
***
NS
NS
WT #1
G93A #1
WT #1
G93A #2
WT #1
G93A #1
WT #1
G93A #2
G+F+I
F+I
I
J
GFP
Metamorph
K
1X
5X
Healthy cell criterion

Fig S2

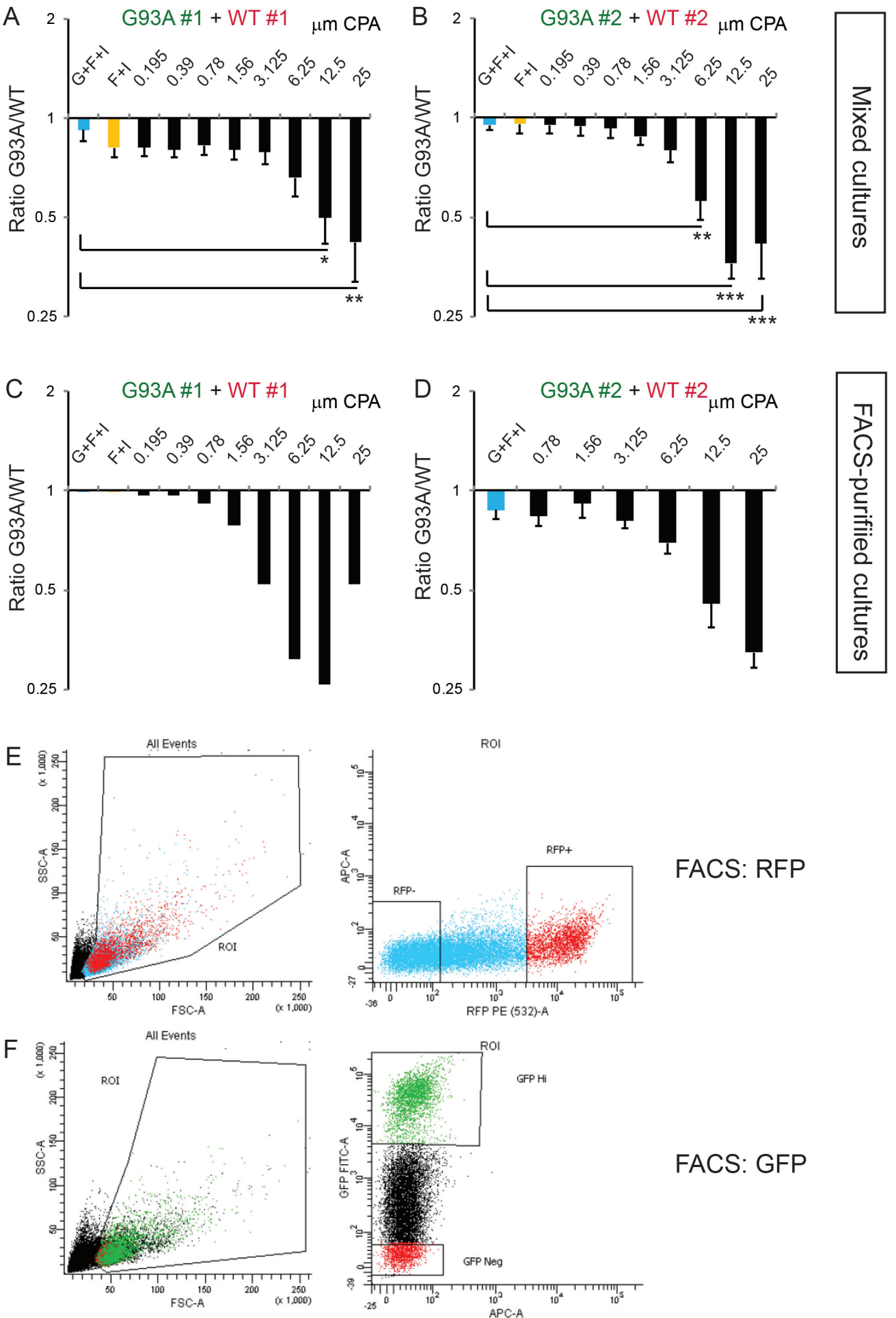
A
G93A #1 + WT #1
µm CPA
Ratio G93A/WT
G+F+I
F+I
0.195
0.39
0.78
1.56
3.125
6.25
12.5
25
B
G93A #2 + WT #2
Mixed cultures
C
G93A #1 + WT #1
D
G93A #2 + WT #2
FACS-purifiied cultures
E
All Events
SSC-A
FSC-A
ROI
RFP-
RFP+
APC-A
RFP PE (532)-A
FACS: RFP
F
GFP Hi
GFP Neg
GFP FITC-A
APC-A
FACS: GFP

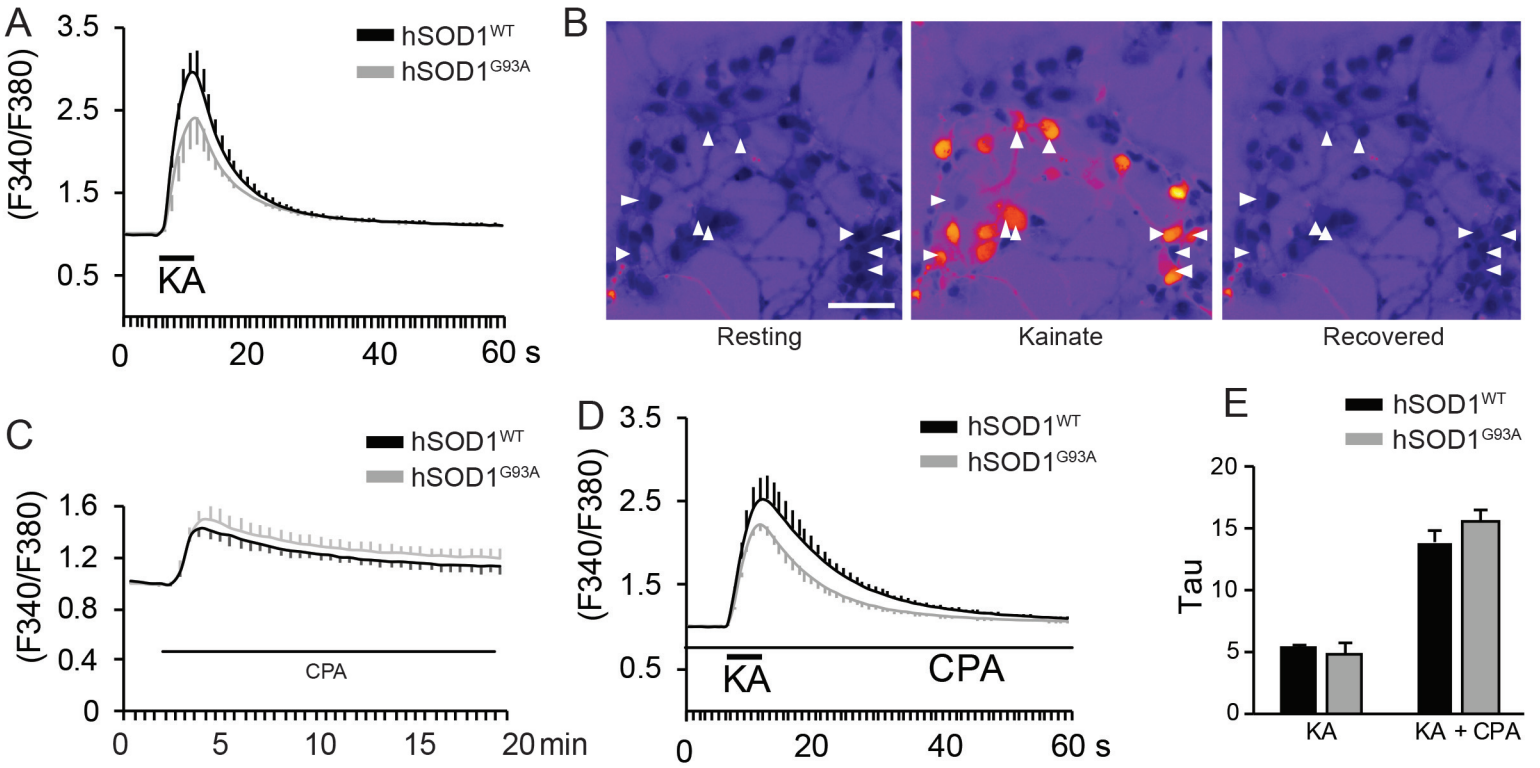
A
3.5
2.5
1.5
0.5
(F340/F380)
hSOD1WT
hSOD1G93A
KA
0
20
40
60 s
B
Resting
Kainate
Recovered
C
hSOD1WT
hSOD1G93A
1.6
1.2
0.8
0.4
0
(F340/F380)
CPA
0
5
10
15
20 min
D
3.5
2.5
1.5
0.5
(F340/F380)
hSOD1WT
hSOD1G93A
KA
CPA
0
20
40
60 s
E
hSOD1WT
hSOD1G93A
20
15
10
5
0
Tau
KA
KA + CPA

Fig. S4

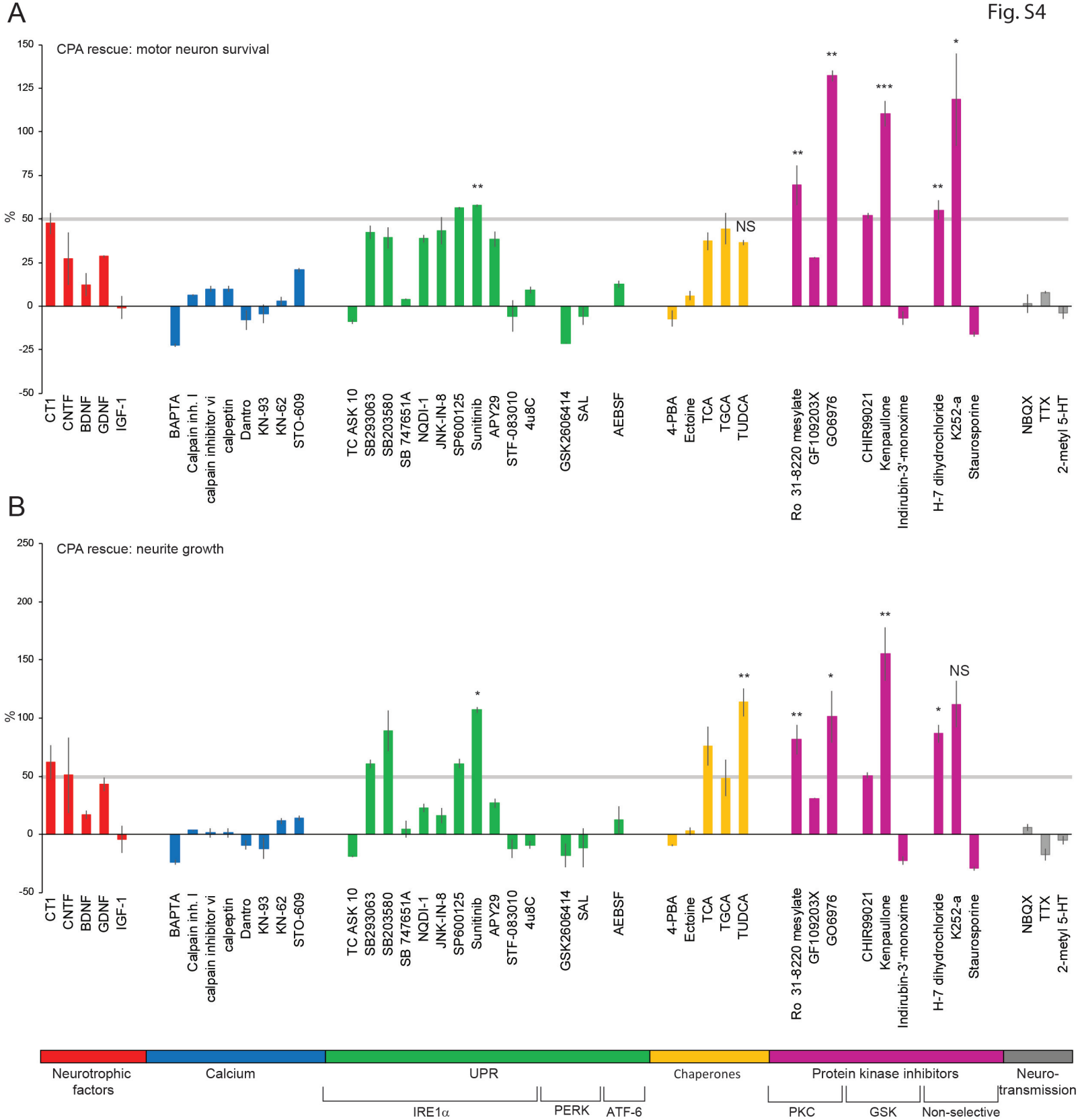
A
CPA rescue: motor neuron survival
%
CT1
CNTF
BDNF
GDNF
IGF-1
BAPTA
Calpain inh. I
calpain inhibitor vi
calpeptin
Dantro
KN-93
KN-62
STO-609
TC ASK 10
SB293063
SB203580
SB 747651A
NQDI-1
JNK-IN-8
SP600125
Sunitinib
APY29
STF-083010
4u8C
GSK2606414
SAL
AEBSF
4-PBA
Ectoine
TCA
TGCA
TUDCA
Ro 31-8220 mesylate
GF109203X
GO6976
CHIR99021
Kenpaullone
Indirubin-3'-monoxime
H-7 dihydrochloride
K252-a
Staurosporine
NBQX
TTX
2-metyl 5-HT
NS
B
CPA rescue: neurite growth
Neurotrophic factors
Calcium
UPR
IRE1α
PERK
ATF-6
Chaperones
Protein kinase inhibitors
PKC
GSK
Non-selective
Neuro-transmission
C
MN survival (%of CTRL)
CTRL
TUDCA
TDCA
TLCA
TCA
UDCA
TCDCA
GUDCA
TGCA
GCDCA
GCA
TMCA
CPA
D
Neurite growth (%of CTRL)

Figure S5

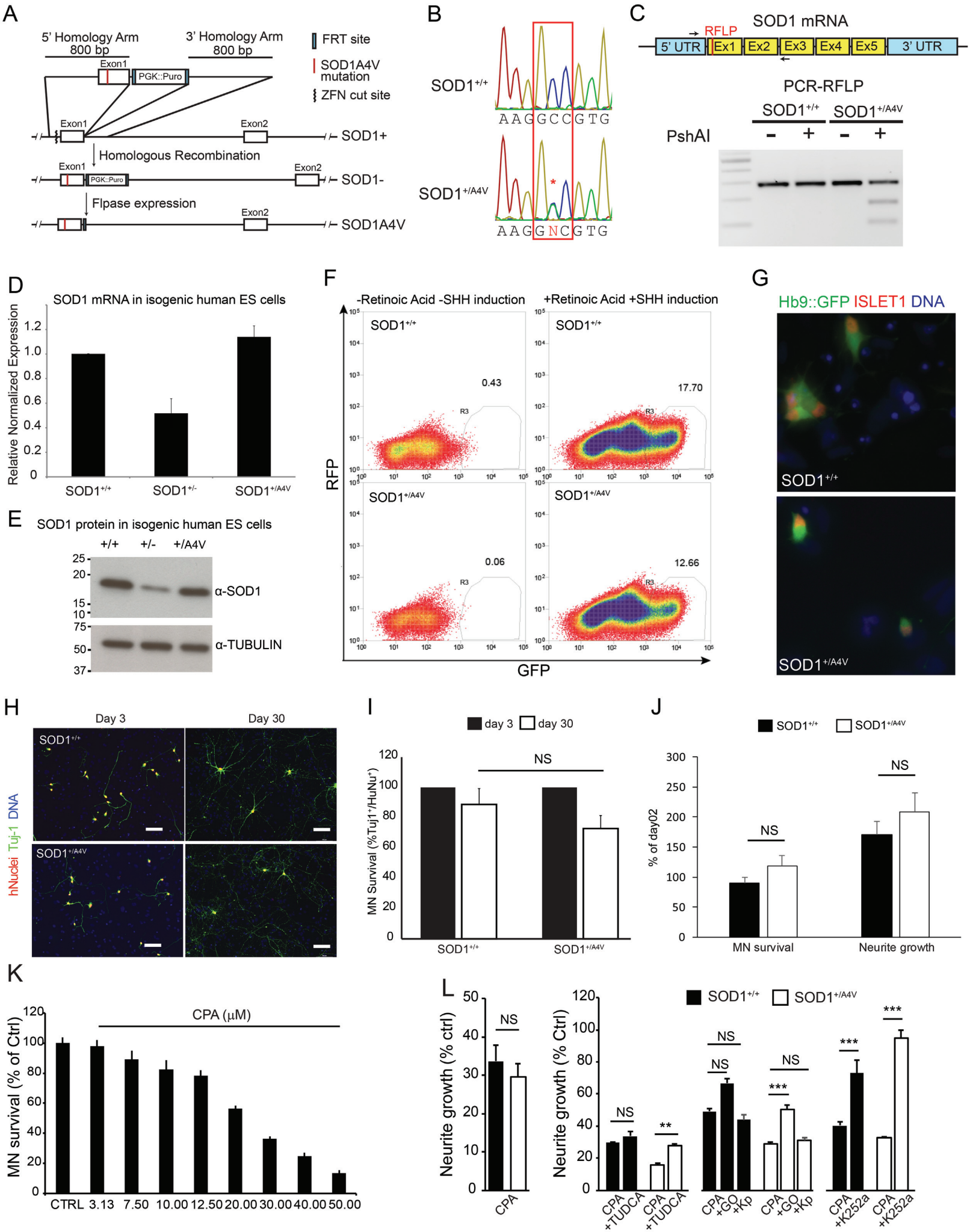
A
5' Homology Arm 800 bp
3' Homology Arm 800 bp
FRT site
SOD1A4V mutation
ZFN cut site
Exon1
PGK::Puro
Exon2
SOD1+
Homologous Recombination
SOD1-
Flpase expression
SOD1A4V
B
SOD1+/+
AAGGCCGTG
SOD1+/A4V
AAGGNCGTG
C
SOD1 mRNA
RFLP
5' UTR
Ex1
Ex2
Ex3
Ex4
Ex5
3' UTR
PCR-RFLP
SOD1+/+
SOD1+/A4V
PshAI
D
SOD1 mRNA in isogenic human ES cells
Relative Normalized Expression
SOD1+/+
SOD1+/-
SOD1+/A4V
E
SOD1 protein in isogenic human ES cells
+/+
+/-
+/A4V
α-SOD1
α-TUBULIN
F
-Retinoic Acid -SHH induction
+Retinoic Acid +SHH induction
RFP
GFP
0.43
17.70
0.06
12.66
R3
G
Hb9::GFP ISLET1 DNA
H
Day 3
Day 30
hNuclei Tuj-1 DNA
I
day 3
day 30
MN Survival (%Tuj1+/HuNu+)
NS
J
% of day02
MN survival
Neurite growth
K
CPA (μM)
MN survival (% of Ctrl)
CTRL 3.13 7.50 10.00 12.50 20.00 30.00 40.00 50.00
L
Neurite growth (% ctrl)
Neurite growth (% Ctrl)
CPA
CPA +TUDCA
CPA +GO +Kp
CPA +K252a

Fig. S6

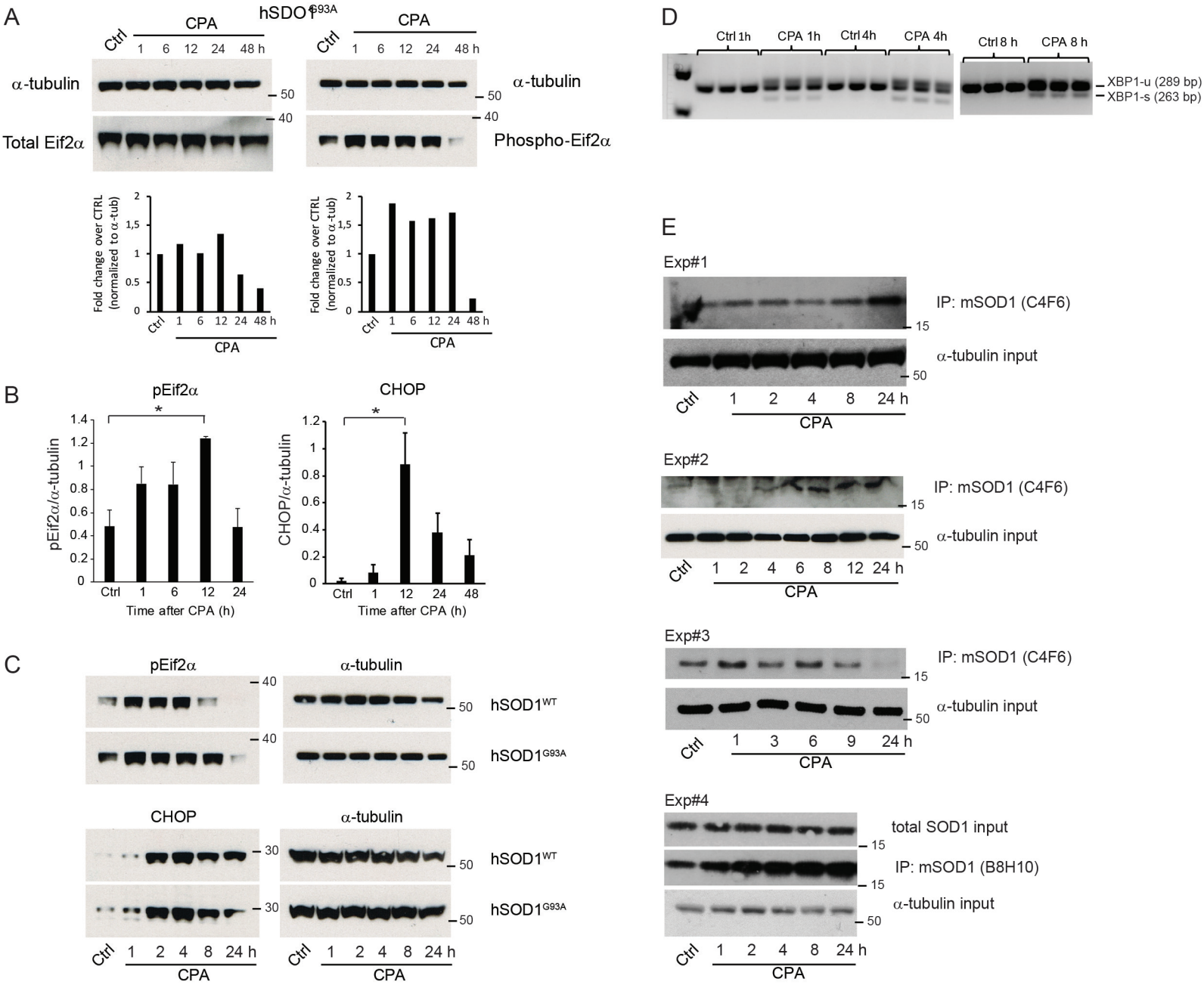
A
hSDO1G93A
CPA
Ctrl
1 6 12 24 48 h
α-tubulin
Total Eif2α
Phospho-Eif2α
50
40
Fold change over CTRL (normalized to α-tub)
B
pEif2α
CHOP
pEif2α/α-tubulin
CHOP/α-tubulin
Time after CPA (h)
C
hSOD1WT
hSOD1G93A
Ctrl 1 2 4 8 24 h
D
Ctrl 1h
CPA 1h
Ctrl 4h
CPA 4h
Ctrl 8 h
CPA 8 h
XBP1-u (289 bp)
XBP1-s (263 bp)
E
Exp#1
Exp#2
Exp#3
Exp#4
IP: mSOD1 (C4F6)
α-tubulin input
total SOD1 input
IP: mSOD1 (B8H10)

Fig. S7

A

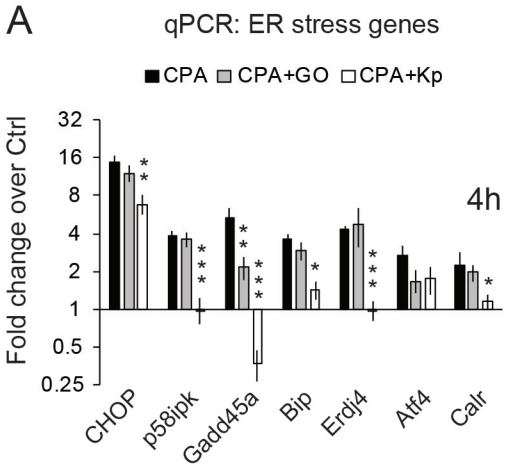

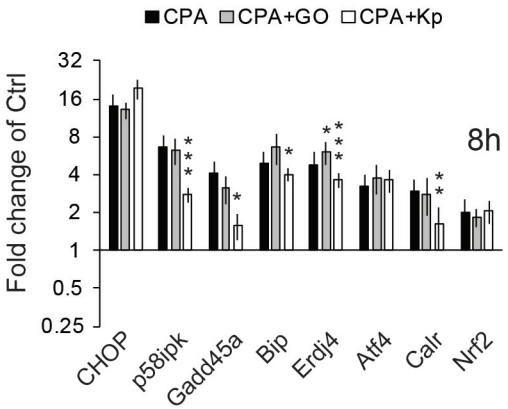

C

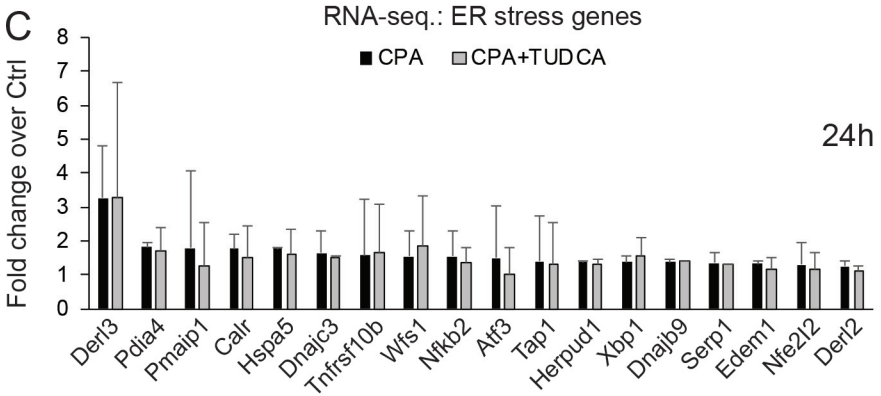

B

Genes	Pathway
CHOP	Induced by ER stress, mediates apoptosis.
p58ipk	Exerts negative feed back loop on PERK pathway
GADD45a	Activates p38/JNK, regulated by-AP1 and ATF-4.
Bip	UPR initiating factor.
Erdj4	ER protein, induced by ER stress, regulates activity of 70kDa heat shock proteins.
Atf4	UPR/PERK pathway.
Calr	Ca^{2}-dependent ER chaperone.
Nrf2	UPR/PERK pathway. Survival promoting transcription factor.

Figure legends

Figure S1. Evaluation of newly derived transgenic ES lines, biochemical analysis of normal- and misfolded SOD1 expression in differentiated cells, and survival motor neuron derived from cell-lines expressing different fluorescent reporters. **(A)** Confocal micrographs showing sections of embryoid bodies from Hb9::RFP hSOD1^{WT} and Hb9::GFP hSOD1^{G93A} stained for motor neuron transcription factors Hb9 and Islet1/2. Scale bar 100 μm. **(B)** Measurements of the overlap between fluorescent reporter protein (FP) and transcriptions factors (TF). Bars denote averages, error bars indicate SEM. **(C-E)** Light microscopy micrographs (**C-D**) and histogram (**E**) showing reporter validation in differentiated new ES lines (two lines for each reporter were differentiated in two separate rounds, results are presented as mean value/reporter). Scale 50 μm. Bars denote means and error bars SEM. **(F)** Cropped images of immunoblots showing expression of total and misfolded (C4F6) SOD1 in untreated motor neuron cultures. P100 spinal cords from WT or SOD1^{G93A} mice were used as controls. The dashed line indicates were the lower image was cropped. **(G)** Immunoblot showing the specificity for the C4F6 andf B8H10 antibodies for misfolded mutant SOD1. **(H)** Motor neuron survival in transgenic hSOD1 WT and G93A cell lines expressing different fluorescent reporters. Survival was assessed in medium (G+F+I) and low (F+I) neurotrophic support in either mixed red-green cultures (red WT #1 + green G93A #1, n=6) or separate cultures (green WT #1, green G93A #2, n=3). Bars denote average, error bars indicate SEM, **p<0.01 ***p<0.001 (Unpaired two-tailed Student's t-test). **(I)** Representative whole-well image of live cells, acquired with the Trophos Plate Runner^{HD}. Scale bar 1 mm. **(J)** Magnification of **(I)** and the result of automated image analysis using Metamorph software. Scale bar 50 μm. **(K)** 'Healthy cell criterion' using presence of a significant neurite to distinguish live cells from fluorescent debris.

Figure S2. Evaluation of CPA toxicity in two independent pair of cell lines, in mixed and FACS-sorted motor neuron cultures. (A-D) Dose response curves for motor neuron survival after CPA treatment in two independent pairs of WT-G93A cell lines (compiled results are shown in Fig. 1D and E). Cultures were either unpurified (**A-B**) or purified using FACS (**C-D**) (**A:** n=5, **B:** n=4, **C:** n=6 culture wells, **D:** n=2). Bars denote average, error bars indicate SEM, *p<0.05, **p<0.01, ***p<0.001 (One-way Anova, *post hoc* Dunnet's multiple comparison test). **(E-F)** Scatter plots showing representative gates for FACS-purification of reporter lines.

Figure S3. Calcium homeostasis in Hb9::RFP hSOD1^{WT} and hSOD1^{G93A} motor neurons exposed to kainic acid and CPA. Biochemical analysis of normal- and misfolded SOD1 expression in differentiated cells. (A) Kainic acid (KA)-induced change in cytoplasmic Ca^{++} was assessed by calculating 340/380 nm ratio in Fura-2 labelled purified hSOD1^{WT} and hSOD1^{G93A} MN cultures. **(B)** Representative example still images of KA-induced calcium transients. Scale bar 50 μm. Images are pseudocolored using the Lookup table 'fire' function in FIJI (increase in calcium is shown in warm colors). The slope of decrease in Fura-2 ratio (Tau) was measured in cultures exposed to kainic acid (KA) in absence or presence of CPA. **(C)** CPA-induced change in cytoplasmic Ca^{++} was assessed by calculating 340/380 nm ratio in Fura-2 labelled purified hSOD1^{WT} and hSOD1^{G93A} MN cultures. **(D)** Kainic acid (KA)-induced change in cytoplasmic Ca^{++} in the presence of CPA was assessed by calculating 340/380 nm ratio in Fura-2 labelled purified hSOD1^{WT} and hSOD1^{G93A} MN cultures (n=5 for WT, n=4 for G93A, for all analyzes). Bars denote average, error bars indicate SEM. **(E)** The slope of decrease in Fura-2 ratio (Tau) was measured in cultures exposed to kainic acid (KA) in absence or presence of CPA.

Figure S4. Selected results from the ER stress rescue screen and mini screen for bile acid derivatives. **(A-B)** Effects of rescue compounds on survival and neurite growth in CPA treated motor neuron cultures. Compounds are subcategorized and color-coded based on their putative mechanisms of action. Bars denote average, error bars indicate SEM (n=3-6 culture wells/compound). The cut-off level for further analysis is indicated by a grey line. Top compounds were compared to CPA only (n=3-6), *p<0.05, **p<0.01, ***p<0.001 (unpaired two-tailed Student's t-test or a Mann-Whitney Rank sum test). **(C-D)** Mini screen for survival (**C**) and neurite rescue (**D**) effects of bile acid derivatives. Each compound was screen in three different concentrations with 5X dilution steps. Bars denote average, error bars indicate SEM (n=3).

Figure S5. Generation of human isogenic cell lines to study aspects of ALS pathogenesis *in vitro*.

(A) Diagram of gene targeting strategy for introduction of the SOD1A4V mutant allele into the SOD1 locus of HUES3 Hb9::GFP. **(B)** Sequencing of the SOD1 locus. **(C)** PCR-RFLP analysis for a unique PshAI restriction site confirmed correct targeting. **(D-E)** qRT-PCR (**D**) and immunoblot (**E**) assays for SOD1 expression in targeted stem cell lines demonstrated reduced levels of the SOD1 transcript and protein levels. **(F)** FACS plots depicting a distinct population of differentiated cells which express the GFP reporter. Differentiated neural cells

not exposed to the MN patterning molecules RA and SAG were used as negative control to gate for green fluorescence. **(G)** Hb9::GFP^{+} cells express the transcription factor Islet1 confirming spinal MN identity. **(H-I)** Cell survival assays in mixed cultures indicate a trend for reduced survival in isogenic human ESC MNs expressing the SOD1^{A4V} variant relative to the isogenic control (**I**). Representative images (**H**) of Human Nuclei and Tuj1 staining at days 3 and 30 (P = 0.09, n= 4). Scale bar 100 μm **(J)** Short term assessment (5 days post dissociation) of MN survival and neurite growth in FACS-purified human isogenic lines, assessed by calcein labelling in live cultures. **(K)** Histogram showing a dose response survival curve for CPA toxicity in purified human SOD1$^{+/A4V}$ ESC MNs. Bars denote average, error bars indicate SEM (n=3 culture wells/concentration). **(L)** Histogram showing neurite growth in purified isogenic human motor neuron cultures. Cells were grown under control conditions, treated with CPA or pretreated with rescue compounds followed by CPA (n=9 for CPA vs. CTRL for both genotypes, (n=3 for rescue compounds for both genotypes). Bars denote average, error bars indicate SEM, *p<0.05, **p<0.01, ***p<0.001 (the effect of CPA was compared between WT vs. ALS MNs, as indicated with a line; the effects of rescue compounds were compared to CPA for each genotype).

Figure S6. Biochemical analysis of UPR mediators and misfolded SOD1.

(A) Western blot showing protein levels of total (left) and phosphorylated Eif2α (right) in cultures treated with CPA. α-tubulin served as loading control. Eif2α bands were quantified and normalized to the loading control, as displayed in the histograms. **(B)** Histograms showing quantification of replicate blots for pEif2α (n=3-7) and CHOP (n= 2-6), and their loading controls (α-tubulin). Bars denote means +/- SEM, *p<0.05 (One-way Anova, *post hoc* Dunnet's multiple comparison test for pEif2α and a Kruskal-Wallis test with Dunn's multiple comparison *post hoc* test for CHOP). **(C)** Western blot showing induction of two UPR markers, pEif2α and CHOP, in hSOD1^{WT} and hSOD1^{G93A} motor neuron cultures. α-tubulin was used as loading control. Please note that hSOD1^{G93A} blot for pEif2α is the same as presented in panel (A). **(D)** Gel image used for quantification of spliced/unspliced XBP1. **(E)** Biological replicate blots for IP lysate and input two antibodies (C4F6 and B8H10) to analyze misfolded SOD1 levels, α-tubulin was used as loading control. Experiment #4 shows that the levels of total SOD1 is unchanged after exposure to CPA.

Figure S7. Analysis of ER stress-associated genes in cultures treated with CPA and rescue compounds.

(A) Histograms showing qPCR results for the ER stress panel for genes that were ≥2-fold upregulated by CPA and ≥2-fold downregulated in hSOD1^{G93A} motor neuron cultures at 4 and/or 8 hours by at least one of the two tested compounds (GO=GÖ6967, Kp=kenpaullone). RNA was extracted from unpurified hSOD1^{G93A} motor neurons (n=3, independent culture dishes). Bars denote average, error bars indicate SEM. CPA was compared to CPA+rescue compounds for each gene and time point, *p<0.05, **p<0.01, ***p<0.001 (One-way Anova, *post hoc* Dunnet's multiple comparison test; or Kruskal-Wallis test with Dunn's multiple comparison *post hoc* test). **(B)** Table showing pathways for the genes displayed in (A). **(C)** Selected results from an RNA-sequence analysis in purified hSOD1^{G93A} motor neurons cultures at 24 hours after exposure to CPA. The histograms shows all ER stress-associated genes that were at least 1.5-fold upregulated by CPA. Bars denote means +/- standard deviation (n=2).

Supplemental table 1

CPA RESCUE SCREEN	% rescue of CPA toxicity	% rescue of CPA toxicity	
Compound	**Cell death**	**Neurite growth**	**Category/pathway**
DCA	20.50911675	33.79013629	Bile acids
CA	17.11925797	67.46744235	Bile acids
HDCA	10.18137182	22.25725601	Bile acids
CDCA	11.22034401	18.22205814	Bile acids
LCA	9.085736241	22.6248862	Bile acids
nor-DCA	14.57261804	19.56389175	Bile acids
HDCA-Me ester	7.110779149	18.92722876	Bile acids
6-Et-CDCA	9.986162197	38.17796374	Bile acids
dehydro-CA	12.31894361	53.84822279	Bile acids
LCA-3-sulfate disodium salt	-2.074362332	6.127374543	Bile acids
ApoCA	1.202390831	-4.777710499	Bile acids
TDCA	10.95840141	65.83163372	Taruine conjugated bile acids and analogues
TLCA	18.97294284	64.49009632	Taruine conjugated bile acids and analogues
TCA	38.08527479	93.68497917	Taruine conjugated bile acids and analogues
UDCA	18.2051565	47.99114566	Taruine conjugated bile acids and analogues
TCDCA	14.28737331	40.5870975	Taruine conjugated bile acids and analogues
GUDCA	9.970678759	41.87969468	Taruine conjugated bile acids and analogues
TGCA	44.55414037	62.09291442	Taruine conjugated bile acids and analogues
GCDCA	2.568580788	4.418783172	Taruine conjugated bile acids and analogues
GCA	23.53008464	35.87867043	Taruine conjugated bile acids and analogues
TMCA	16.10051109	31.5368093	Taruine conjugated bile acids and analogues
Ectoine	5.031032977	4.253494542	Chemical chaperons
Butylated hydroxyanisole	1.354844525	-0.941491828	Chemical chaperons
Ferrostatin-1	2.79356048	-2.344252599	Chemical chaperons
AL8810	1.258232698	-2.05527542	Chemical chaperons
PBA	-41.56239575	-11.70826719	Chemical chaperons
AK1	-23.86319535	-30.83271417	PDI inhibitors
AK2	1.337184819	-3.257907284	PDI inhibitors
AK3	-13.69763943	-15.12140467	PDI inhibitors
AK4	-39.65076275	-46.47310177	PDI inhibitors
AK5	-23.68718212	2.312235213	PDI inhibitors
AK6	3.063364798	2.312235213	PDI inhibitors
AK7	-7.303783075	-11.93026762	PDI inhibitors
AK8	-27.88593481	-36.62835997	PDI inhibitors
AK9	-0.382896758	-2.05527542	PDI inhibitors
AK10	0.714780145	-10.31330492	PDI inhibitors
AK11	1.17828197	-3.620404836	PDI inhibitors
AK12	-11.97948204	-17.65611204	PDI inhibitors
AK13	9.871088291	16.26285303	PDI inhibitors
AK14	0.788806148	1.478837654	PDI inhibitors
AK15	2.542958577	2.436655716	PDI inhibitors
H89	-30.09836713	-22.30613359	PKA inhibtor
Ro 32-0432	69.45362016	81.40427339	PKC pathway
Go 6976	132.071419	164.4046336	PKC pathway

Phorbol-12-Myristate-13-Acetate (PMA)	27.1651683	27.55476829	PKC pathway
SRI22782	-10.20702158	18.68101413	PKC pathway
H-7 dihydrochloride	65.1027217	86.7200762	PKC pathway
Staurosporine	20.47359662	14.17999838	PKC pathway
GF109203X	27.85088299	30.94050956	PKC pathway
Ro 31-8220 mesylate	69.45362016	81.40427339	PKC pathway
Calpain inh. I	6.32809798	3.560770737	Calcium signalling
calpain inh. vi	9.877545437	3.897137092	Calcium signalling
calpeptin	3.098288729	0.67757198	Calcium signalling
Dorsomorphin dihydrochloride	6.73967196	27.84365219	Calcium signalling
KN-93	-4.231510218	-9.039734584	Calcium signalling
KN-62	3.130314662	-4.057607419	Calcium signalling
SC 79	-12.66320348	24.67689953	Calcium signalling
ML-7	-16.018605	-14.00783075	Calcium signalling
BAPTA-am	-22.4076638	-23.85843413	Calcium signalling
Dantro	-7.951848422	-9.099424947	Calcium signalling
STO-609	20.72023166	14.10316415	Calcium signalling
SB203580	42.38514236	60.62167911	P38 pathway
SB293063	39.23672175	88.75752601	P38 pathway
SB747651A	19.57562965	7.742367164	P38 pathway
TC ASK 10	-1.618735713	-2.830851895	UPR: IRE1a pathway
NQDI-1	38.83991819	14.22598976	UPR: IRE1a pathway
JNK-IN-8	43.27201114	16.24361567	UPR: IRE1a pathway
SP600125	56.27881783	60.92493308	UPR: IRE1a pathway
APY29	57.75930514	106.9694934	UPR: IRE1a pathway
4u8C	9.303566151	-0.004912081	UPR: IRE1a pathway
STF-083010	9.975897399	3.15447713	UPR: IRE1a pathway
GSK2606414	21.91490255	0.731015109	UPR: PERK pathway
SAL	-5.720293345	-11.87407306	UPR: PERK pathway
AEBSF	12.53726409	12.53726409	UPR: ATF-6 pathway
K-252a	118.4447322	112.0067487	MLK pathway
Indirubin-3'-monoxime	1.508853123	-0.051027126	GSK3/CDK5 pathway
Roscovitine	5.759798441	50.80843357	GSK3/CDK5 pathway
Kenpaullone	110.5319404	155.2520568	GSK3/CDK5 pathway
CHIR99021	51.87279329	50.56491705	GSK3/CDK5 pathway
PD184352	-24.33699154	-16.25729121	MEK/ERK pathway
BRD7386	-0.290118349	-4.395083851	MEK/ERK pathway
TTX	19.50429801	0.62468452	Neurotransmission
2-metyl 5-hydroxy tryptamine	0.767196361	3.779436554	Neurotransmission
Guanabenz acetate salt	-5.953047358	-1.698662404	Neurotransmission
NBQX	1.544616023	5.665939173	Neurotransmission
DOPA	2.064118232	38.55848623	Neurotransmission
PMA	-5.730983276	25.50379088	Neurotransmission
Gambogic amide	2.750107789	39.31132329	Neurotransmission
CT1	47.45118857	62.31697159	Neurotrophic factors
CNTF	27.2134856	50.77820319	Neurotrophic factors
BDNF	12.36232474	16.59337082	Neurotrophic factors
GDNF	28.46762539	43.13787768	Neurotrophic factors
IGF-1	4.009108083	0.416651788	Neurotrophic factors
TRIM	13.72176778	53.0837837	NO signaling
CD253 (TRAIL) Antibody	-1.02268982	28.50003468	TNF superfamily & apoptosis
Caspase-8 inhibitor II	2.170111685	45.44852287	TNF superfamily & apoptosis
Sorafenib	-8.33727539	-5.065283411	Tyrosine kinase inhibitors
Sunitinib	57.75930514	106.9694934	Tyrosine kinase inhibitors
Ehop-016	-58.41396916	-44.41603223	Rac pathway
ZCL 278	3.473221912	13.44168678	Rac pathway
Fasudil	8.602455737	18.08080674	Rho pathway

PF-4708671	-11.45136888	-16.50140601	RSK inhibitor
SL0101	28.18089475	88.93617474	RSK inhibitor
PD407 5	25.41529778	NA	Chk1 pathway
NSC632839	3.12881176	10.71355041	Isopeptidase inh.
Phenazine methosulfate	-43.39544535	-18.42018807	Miscellaneous
Phenethyl isothiocyanate	-29.4794646	-5.868143127	Miscellaneous

Table S1. A screen for rescue of CPA toxicity

A list of compounds tested for their ability to reverse CPA-induced MN toxicity and/or neurite retraction. Compounds are subdivided based on putative pathways or mechanisms of action. Rescue effects are expressed as % reversal of the CPA-effect for survival and neurite growth. for the best time point (24 or 48 hrs post CPA) and concentration tested. Values either represent the averages of replicate culture wells. or from independent experiments for compounds evaluated in follow-up experiments.